Computers and Structures 254 (2021) 106531

Contents lists available at ScienceDirect

Computers and Structures

journal homepage: www.elsevier.com/locate/compstruc

Transient wave propagations with the Noh-Bathe scheme and the spectral element method

Pooya Zakian [a], Klaus-Jürgen Bathe [b,*]

[a] Department of Civil Engineering, Faculty of Engineering, Arak University, Arak, Iran
[b] Massachusetts Institute of Technology, Cambridge, MA 02139, United States

ARTICLE INFO

Article history:
Received 16 December 2020
Accepted 9 March 2021

Keywords:
Spectral element method
Noh-Bathe explicit time integration
Central difference explicit time integration
Spatial and temporal dispersion errors
CFL numbers
Wave propagation

ABSTRACT

The spectral elements of the Lobatto family provide desirable characteristics of convergence and accuracy using a diagonal mass matrix in dynamic analysis. These characteristics might be expected to render the spectral element method with the use of an explicit time integration scheme effective for the transient analysis of wave propagations. In this paper we study the use of the central difference method and the recently proposed Noh-Bathe method for explicit time integration in the use of the spectral finite element method. The Noh-Bathe scheme is a second-order accurate procedure with small solution errors in the required frequency range while suppressing spurious high frequencies. We calculate appropriate CFL numbers for the time integrations and give an analysis of the dispersion errors for different orders of spectral elements. Finally, we demonstrate the capabilities of the Noh-Bathe scheme compared to the central difference method through the solution of several numerical examples of wave propagations.

1. Introduction

The spectral element method, also known as the spectral finite element method, is based on two numerical techniques, namely spectral methods and finite element methods, and offers some of the flexibility of the finite element method with the accuracy of spectral methods. A popular family of spectral elements is based on using Lagrange polynomials expressed in terms of Lobatto collocation points and Gauss-Lobatto-Legendre numerical integration. This approach results into a diagonal mass matrix for dynamic analysis [1,2].

In contrast to the finite element method, the spectral element method uses unequally spaced nodes whose locations are the zeros of the interpolation polynomials. This feature can diminish large oscillations of the approximating polynomials close to edges. The exponential form of convergence using the diagonal mass matrix is a reason why the method is extensively used in the analyses of wave propagations in computational seismology [3–10]. As in the traditional finite element method, the discretized equations of motion are solved using a direct time integration method. Usually, the accuracy of a time integration scheme when used with a spatial discretization is measured by the numerical dispersion and dissipation of the solution technique, see, for example, considering finite element analyses Refs. [11–17] and considering the spectral element method Refs. [18–23]. However, in finite element wave propagation analyses usually low-order elements are used [12] and it is important to assess in how far spectral elements, which are of higher-order, are effective. Then an appropriate Courant, Friedrichs, Lewy (CFL) number needs to be used [12], but there seems to be no simple relationship to establish an effective CFL for higher-order spectral elements.

There are two approaches for direct time integration, that is, explicit and implicit schemes are used. A time integration method is implicit when it requires the factorization of an effective stiffness (or mass) matrix and is otherwise explicit. Both approaches can be used for transient wave propagation solutions. An unconditionally stable implicit method uses less time steps but requires a much larger computational effort per step. This solution effort is particularly large when the bandwidth of the effective stiffness matrix is large [12,24]. An explicit method uses a much larger number of steps, but since no effective stiffness matrix is employed, the computational effort is much smaller per time step. Depending on the problem solved, an explicit or implicit time integration may be computationally more effective.

Using the spectral element method, explicit time integration methods are commonly employed in the analysis of wave propagations [3,9,10,25–28]. This is a natural approach to use, since the mass matrix used is diagonal and the bandwidth of the effective stiffness matrix would be large, in fact so large that frequently a

* Corresponding author.
E-mail address: kjb@mit.edu (K.J. Bathe).

https://doi.org/10.1016/j.compstruc.2021.106531
0045-7949/

solution using an implicit time integration scheme is computationally out of reach. In contrast, as in traditional finite element solutions, in the explicit time integration, element-by-element assemblage of the solution vectors and parallel computing are employed [12]. However, since explicit methods are not unconditionally stable, the time step must be chosen to satisfy the applicable stability limit, which depends on the integration scheme, the element type, the element "size", the mesh and the physical aspects of the wave propagation problem.

In order to reduce the solution errors, higher-order spatial discretizations appear to be attractive, as found using enriched overlapping finite elements [17,29]. With the dispersion error due to the spatial discretization reduced, the errors induced by the time integration should also be small and need to be evaluated [29]. An effective time integration scheme imposes numerical dissipation to suppress high frequency spurious modes while giving good accuracy in the integration of the modes of the finite element model that accurately represent the "exact" modes of the continuum [12,15,30].

An explicit method widely used for wave propagation solutions, also in seismology, is the central difference method [1,3,6,9,10,26,28,31]. It has the largest time step stability limit compared to other second-order accurate explicit methods. However, the central difference method has two main shortcomings: firstly, being a non-dissipative technique, it does not provide numerical damping for the spurious modes to be suppressed and, secondly, the method requires the factorization of a banded matrix if a non-diagonal damping matrix is used, like obtained with Rayleigh damping [12].

There are a number of dissipative explicit methods, in particular those proposed by Newmark [32], Chung and Lee [33], Hulbert and Chung [34], Zhai [35], Tchamwa and Wielgosz [36] and Noh and Bathe [15]. The Newmark explicit and the Zhai explicit methods are categorized as first-order accurate methods with the desired high frequency dissipation but these techniques also decrease the solution accuracy in the low frequency range. The other above-mentioned methods are dissipative in the high-frequency range and second-order accurate, but, except for the Noh-Bathe scheme, provide less accurate solutions than the first order accurate Tchamwa-Wielgosz method. The Noh-Bathe scheme provides effective numerical damping for the spurious modes to be suppressed and also does not require, for effectiveness, the use of a non-banded damping matrix, hence can directly be used with Rayleigh damping [15].

In addition to using an effective time integration, the use of an effective spatial discretization is necessary. Higher-order finite elements with the p-method have been used for many years in structural analysis but have finally found limited applications [37,38], the traditional low-order elements have much prevailed in industrial applications. However, recently the overlapping finite elements with enrichments have shown much promise, albeit in implicit time integration [17,29]. These are in essence, elements of higher-order with element interpolations and degrees of freedom designed to solve wave propagation problems. Given these results obtained with higher-order elements, it is valuable to study the use of spectral elements in transient wave propagations with explicit time integration.

Our objective in this paper is to study and use the Noh-Bathe explicit scheme with the spectral element method for the analysis of wave propagations, to identify the effectiveness in comparison to the use of the central difference scheme, and to evaluate whether the higher-order spectral elements can be efficiently used in solving wave propagation problems.

For this purpose, we perform an analysis of the spatial and the temporal dispersion errors for different orders of spectral elements and establish an appropriate CFL number for each element for use of the central difference and Noh-Bathe schemes. To illustrate and compare the performance of the Noh-Bathe and central difference schemes when using the spectral element method, for different element orders, CFL numbers and mesh densities, we give the solutions of some numerical examples of wave propagations.

2. Preliminaries on the spectral element method

The spectral element method is a numerical method with characteristics of spectral methods and finite element methods. The method was developed for transient analyses to overcome numerical errors due to period elongation and amplitude decay, known as numerical dispersion and dissipation. We consider here the Lobatto family of the spectral element method, in which the Lobatto collocation points are used to construct the interpolation functions and Gauss-Lobatto-Legendre quadrature is utilized to compute the element matrices. Hence the mass matrix is diagonal [28,39,40].

For a displacement field $\mathbf{u}(x,y,t)$ in two-dimensional domains, the equations of motion for elastic wave propagation are

$$\rho\ddot{\mathbf{u}} = \nabla\cdot\boldsymbol{\tau} + \mathbf{f} \tag{1}$$

in which ρ, $\boldsymbol{\tau}$ and $\mathbf{f}$ are the mass density, stress tensor and body force vector, respectively. The governing equation is subjected to two types of boundary conditions, the Dirichlet boundary condition,

$$\mathbf{u} = \mathbf{u}^{S_D} \tag{2}$$

and the Neumann boundary condition

$$\boldsymbol{\tau}\cdot\mathbf{n} = \mathbf{f}^{S_N} \tag{3}$$

where $\mathbf{n}$ denotes the unit normal vector on the boundary S_N. Using the principle of virtual work, we obtain [12]

$$\int_V \bar{\boldsymbol{\varepsilon}}^T\boldsymbol{\tau}\ \mathrm{dV} + \int_V \rho\ \bar{\mathbf{u}}^T\ddot{\mathbf{u}}\,\mathrm{dV} = \int_V \bar{\mathbf{u}}^T\mathbf{f}\ \mathrm{dV} + \int_{S_N} \bar{\mathbf{u}}_{S_N}^T\mathbf{f}_{S_N}\mathrm{dS} \tag{4}$$

in which $\bar{\mathbf{u}}$ and $\bar{\boldsymbol{\varepsilon}}$ indicate the virtual displacement and the corresponding virtual strain, respectively. Also, $\mathbf{f}_{S_N}$ are the imposed surface tractions.

Discretizing Eq. (4), we arrive at the following matrix form of the governing equations

$$\mathbf{M}\ddot{\mathbf{U}} + \mathbf{C}\dot{\mathbf{U}} + \mathbf{K}\mathbf{U} = \mathbf{R} \tag{5}$$

where $\mathbf{M}$, $\mathbf{C}$ and $\mathbf{K}$ are the mass, damping and stiffness matrices, respectively. Also, $\ddot{\mathbf{U}}$, $\dot{\mathbf{U}}$, $\mathbf{U}$ and $\mathbf{R}$ are the acceleration, velocity, displacement and force vectors varying with time. The constitutive law, strain–displacement and interpolation relations are defined as

$$\boldsymbol{\tau} = \mathbf{C}\boldsymbol{\varepsilon}, \quad \boldsymbol{\varepsilon} = \mathbf{B}\mathbf{U}, \quad \mathbf{u} = \mathbf{H}\mathbf{U} \tag{6}$$

For a two-dimensional spectral element of order n, we have the following interpolation function matrix with ℓ nodes

$$\mathbf{H} = \begin{bmatrix} h_1 & 0 & h_2 & 0 & \cdots & h_{\ell-1} & 0 & h_\ell & 0 \\ 0 & h_1 & 0 & h_2 & \cdots & 0 & h_{\ell-1} & 0 & h_\ell \end{bmatrix}_{2\times 2\ell} \tag{7}$$

in which $\ell = (n+1)(n+1)$, and Lobatto collocation points are used for the Lagrange polynomials in $\mathbf{H}$.

In the isoparametric formulation, the Lobatto points are the roots of the following equation for each dimension

$$(1-r^2)P'_{n-1}(r) = 0 \tag{8}$$

such that $P'_{n-1}(r)$ represents the first derivative of the Legendre polynomial of degree n-1 usually obtained from the Rodrigues relation [2,28]

$$P'_k(r) = \frac{1}{2^{k+1}(k+1)!}\frac{\mathrm{d}^{k+2}}{\mathrm{d}r^{k+2}}(r^2-1)^{k+1} \tag{9}$$

As an example, the Lagrange interpolation functions of a 3rd order quadrilateral spectral element with 16 nodes (see Fig. 1) are [39]:

$$\begin{aligned}
h_1 &= \tfrac{1}{64}(5r^2-1)(5s^2-1)(r-1)(s-1),\\
h_2 &= -\tfrac{\sqrt{5}}{64}(5r-\sqrt{5})(5s^2-1)(r^2-1)(s-1),\\
h_3 &= \tfrac{\sqrt{5}}{64}(5r+\sqrt{5})(5s^2-1)(r^2-1)(s-1),\\
h_4 &= -\tfrac{1}{64}(5r^2-1)(5s^2-1)(r+1)(s-1),\\
h_5 &= -\tfrac{\sqrt{5}}{64}(5r^2-1)(5s-\sqrt{5})(r-1)(s^2-1),\\
h_6 &= \tfrac{5}{64}(5r-\sqrt{5})(5s-\sqrt{5})(r^2-1)(s^2-1),\\
h_7 &= -\tfrac{5}{64}(5r+\sqrt{5})(5s-\sqrt{5})(r^2-1)(s^2-1),\\
h_8 &= \tfrac{\sqrt{5}}{64}(5r^2-1)(5s-\sqrt{5})(r+1)(s^2-1),\\
h_9 &= \tfrac{\sqrt{5}}{64}(5r^2-1)(5s+\sqrt{5})(r-1)(s^2-1),\\
h_{10} &= -\tfrac{5}{64}(5r-\sqrt{5})(5s+\sqrt{5})(r^2-1)(s^2-1),\\
h_{11} &= \tfrac{5}{64}(5r+\sqrt{5})(5s+\sqrt{5})(r^2-1)(s^2-1),\\
h_{12} &= -\tfrac{\sqrt{5}}{64}(5r^2-1)(5s+\sqrt{5})(r+1)(s^2-1),\\
h_{13} &= -\tfrac{1}{64}(5r^2-1)(5s^2-1)(r-1)(s+1),\\
h_{14} &= \tfrac{\sqrt{5}}{64}(5r-\sqrt{5})(5s^2-1)(r^2-1)(s+1),\\
h_{15} &= -\tfrac{\sqrt{5}}{64}(5r+\sqrt{5})(5s^2-1)(r^2-1)(s+1),\\
h_{16} &= \tfrac{1}{64}(5r^2-1)(5s^2-1)(r+1)(s+1).
\end{aligned} \tag{10}$$

We should note the uneven spacing of the nodal points of the element, as depicted in Fig. 1.

3. Explicit time integration methods

In this section, we briefly state the governing solution steps used in the central difference and Noh-Bathe explicit schemes.

3.1. Central difference scheme

The fundamental solution steps of the central difference method (CDM) are as follows [12]:

Step 1: Form mass matrix **M**, damping matrix **C**, and stiffness matrix **K** (but see comment below regarding **K**)

Step 2: Initialize displacement vector ${}^0\mathbf{U}$, velocity vector ${}^0\dot{\mathbf{U}}$, and acceleration vector ${}^0\ddot{\mathbf{U}}$.

Step 3: Select time step size $\Delta t \leqslant \Delta t_{cr}$, and calculate integration constants as given by:

$$a_0 = \frac{1}{\Delta t^2};\quad a_1 = \frac{1}{2\Delta t};\quad a_2 = 2a_0;\quad a_3 = \frac{1}{a_2} \tag{11}$$

Step 4: Calculate ${}^{-\Delta t}\mathbf{U} = {}^0\mathbf{U} - \Delta t\,{}^0\dot{\mathbf{U}} + a_3\,{}^0\ddot{\mathbf{U}}$.

Step 5: Form effective mass matrix as $\hat{\mathbf{M}} = a_0\mathbf{M} + a_1\mathbf{C}$.

Step 6: Calculate effective load vector at time t, as follows:

$${}^t\hat{\mathbf{R}} = {}^t\mathbf{R} - (\mathbf{K} - a_2\mathbf{M})\,{}^t\mathbf{U} - (a_0\mathbf{M} - a_1\mathbf{C})\,{}^{t-\Delta t}\mathbf{U} \tag{12}$$

Step 7: Solve the following equation for displacement vector at time $t+\Delta t$:

$$\hat{\mathbf{M}}\,{}^{t+\Delta t}\mathbf{U} = {}^t\hat{\mathbf{R}} \tag{13}$$

Step 8: If necessary, calculate acceleration and velocity vectors at time t as follows:

$$\begin{aligned}
{}^t\ddot{\mathbf{U}} &= a_0({}^{t-\Delta t}\mathbf{U} - 2\,{}^t\mathbf{U} + {}^{t+\Delta t}\mathbf{U})\\
{}^t\dot{\mathbf{U}} &= a_1(-{}^{t-\Delta t}\mathbf{U} + {}^{t+\Delta t}\mathbf{U})
\end{aligned} \tag{14}$$

Step 9: Continue with Step 6, but once all time steps have been calculated, the process is terminated.

Since the **K**-matrix is only on the right-hand side in Eq. (13), assuming no stiffness-proportional damping, the product $\mathbf{K}\,{}^t\mathbf{U}$ can in practice be calculated element-by-element, then the complete stiffness matrix is not assembled [12]. But we note that in Eq. (13) the damping matrix is on the left-hand side of the equation, hence if a banded matrix is used (like in Rayleigh damping, $\mathbf{C} = \alpha\mathbf{M} + \beta\mathbf{K}$ where α, β are constants) each solution step is very expensive, like in an implicit time integration, and too expensive for an explicit integration, in particular for higher-order elements which provide a large bandwidth in the governing equations.

3.2. Noh-Bathe scheme

The fundamental solution steps of the Noh-Bathe method (NBM) are as follows [15]:

Step 1: Form mass matrix **M**, damping matrix **C**, and stiffness matrix **K** (but see comment below regarding **K**)

Step 2: Initialize displacement vector ${}^0\mathbf{U}$, velocity vector ${}^0\dot{\mathbf{U}}$, and acceleration vector ${}^0\ddot{\mathbf{U}}$.

Step 3: Select time step size $\Delta t \leqslant \Delta t_{cr}$ and p ($p = 0.54$ is recommended), and calculate integration constants as given by:

$$\begin{aligned}
&q_1 = \tfrac{1-2p}{2p(1-p)};\quad q_2 = \tfrac{1}{2} - pq_1;\quad q_0 = -q_1 - q_2 + \tfrac{1}{2};\quad a_0 = p\Delta t;\\
&a_1 = \tfrac{1}{2}(p\Delta t)^2;\quad a_2 = \tfrac{a_0}{2};\quad a_3 = (1-p)\Delta t;\quad a_4 = \tfrac{1}{2}((1-p)\Delta t)^2;\\
&a_5 = q_0 a_3;\quad a_6 = (\tfrac{1}{2} + q_1)a_3;\quad a_7 = q_2 a_3
\end{aligned} \tag{15}$$

Step 4-1: Calculate displacement and effective load vectors at time $t + p\Delta t$, as follows:

$$\begin{aligned}
{}^{t+p\Delta t}\mathbf{U} &= {}^t\mathbf{U} + a_0\,{}^t\dot{\mathbf{U}} + a_1\,{}^t\ddot{\mathbf{U}}\\
{}^{t+p\Delta t}\tilde{\mathbf{R}} &= (1-p)\,{}^t\mathbf{R} + p\,{}^{t+\Delta t}\mathbf{R}\\
{}^{t+p\Delta t}\hat{\mathbf{R}} &= {}^{t+p\Delta t}\tilde{\mathbf{R}} - \mathbf{K}\,{}^{t+p\Delta t}\mathbf{U} - \mathbf{C}({}^t\dot{\mathbf{U}} + a_0\,{}^t\ddot{\mathbf{U}})
\end{aligned} \tag{16}$$

Step 4-2: Solve the following equation for acceleration vector at time $t + p\Delta t$:

$$\mathbf{M}\,{}^{t+p\Delta t}\ddot{\mathbf{U}} = {}^{t+p\Delta t}\hat{\mathbf{R}} \tag{17}$$

Step 4-3: Calculate velocity vector at time $t + p\Delta t$ as follows:

$${}^{t+p\Delta t}\dot{\mathbf{U}} = {}^t\dot{\mathbf{U}} + a_2({}^t\ddot{\mathbf{U}} + {}^{t+p\Delta t}\ddot{\mathbf{U}}) \tag{18}$$

Step 5-1: Calculate displacement and effective load vectors at time $t + \Delta t$, as follows:

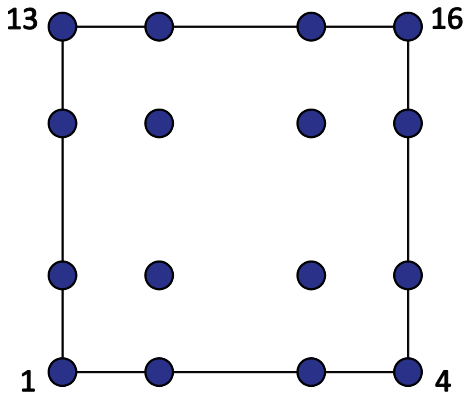

Fig. 1. A 3rd order spectral element.

$$
\begin{aligned}
{}^{t+\Delta t}\mathbf{U} &= {}^{t+p\Delta t}\mathbf{U} + a_3\,{}^{t+p\Delta t}\dot{\mathbf{U}} + a_4\,{}^{t+p\Delta t}\ddot{\mathbf{U}} \\
{}^{t+\Delta t}\hat{\mathbf{R}} &= {}^{t+\Delta t}\mathbf{R} - \mathbf{K}\,{}^{t+\Delta t}\mathbf{U} - \mathbf{C}({}^{t+p\Delta t}\dot{\mathbf{U}} + a_3\,{}^{t+p\Delta t}\ddot{\mathbf{U}})
\end{aligned} \tag{19}
$$

Step 5-2: Solve the following equation for acceleration vector at time $t+\Delta t$:

$$
\mathbf{M}\,{}^{t+\Delta t}\ddot{\mathbf{U}} = {}^{t+\Delta t}\hat{\mathbf{R}} \tag{20}
$$

Step 5-3: Calculate velocity vector at time $t+\Delta t$ as follows:

$$
{}^{t+\Delta t}\dot{\mathbf{U}} = {}^{t+p\Delta t}\dot{\mathbf{U}} + a_5\,{}^{t}\ddot{\mathbf{U}} + a_6\,{}^{t+p\Delta t}\ddot{\mathbf{U}} + a_7\,{}^{t+\Delta t}\ddot{\mathbf{U}} \tag{21}
$$

Step 6: Continue with Step 4-1, but once all time steps have been calculated, the process is terminated.

We note that again there is no need to assemble a complete stiffness matrix **K**, in addition, in Eq. (17) the damping matrix does not appear on the left-hand side of the equation, hence a banded damping matrix (as for Rayleigh damping) can directly be used effectively in the time integration.

4. Dispersion analysis

In this section, we analyze the dispersion errors arising from the spatial discretization. Spectral elements with orders ranging from 3 to 8 seem very popular for the solution of transient wave propagations [27]. Therefore, we focus on these orders of elements for the solution of

$$
\frac{\partial^2 u}{\partial t^2} - c^2\nabla^2 u = 0 \tag{22}
$$

subject to appropriate boundary and initial conditions. Here u is the field variable (we refer to it as a displacement below) and c is the exact wave velocity. The spectral element discretization yields, as in traditional finite element analysis,

$$
\mathbf{M}\ddot{\mathbf{U}} + \mathbf{K}\mathbf{U} = \mathbf{0} \tag{23}
$$

where

$$
\begin{aligned}
\mathbf{M}^{(m)} &= \int_{V^{(m)}} \mathbf{H}^{(m)^{\mathrm{T}}}\mathbf{H}^{(m)}\,\mathrm{d}V^{(m)} \\
\mathbf{K}^{(m)} &= c^2\int_{V^{(m)}} (\nabla\mathbf{H}^{(m)})^{\mathrm{T}}(\nabla\mathbf{H}^{(m)})\,\mathrm{d}V^{(m)}
\end{aligned} \tag{24}
$$

and $\mathbf{K}^{(m)}$ and $\mathbf{M}^{(m)}$ are the stiffness and mass matrices for the m'th element with volume $V^{(m)}$, respectively. In these equations, **H** is the element displacement interpolation matrix. In the finite element or spectral element solution of Eq. (22) we have only one degree of freedom (DOF) per node. We should note that although we give in Eq. (24) the equations for the consistent mass matrix [12], when used for the Lobatto family of spectral elements with Gauss-Lobatto-Legendre numerical integration, the mass matrix is automatically diagonal.

4.1. Spatial dispersion of spectral elements

In two-dimensional analysis, the general solution of Eq. (22) takes the form

$$
{}^{t}_{x,y}u = A_k e^{i(kx\cos(\theta)+ky\sin(\theta)-\omega t)} \tag{25}
$$

where x and y are the coordinate values of a point in the (x,y) system placed at the mid-node of the patch, see Fig. 2, θ is the direction of wave travel, k is the wave number, A_k is a constant and ω is the frequency (rad/s).

For finding the dispersion relationship, a structured homogeneous mesh of equal-size elements is considered. We show in Fig. 2 four typical elements constituting a patch. The displacement of the central node is obtained in terms of the displacements at the nodes around it. For the uniform mesh shown in Fig. 2, we define $x = n_x h,\ y = n_y h$, where h is the "element length" and n_x, n_y are

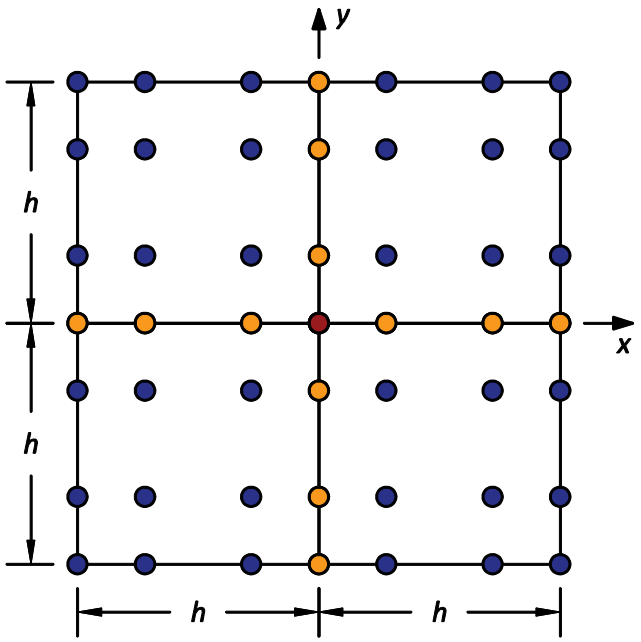

Fig. 2. A mesh (patch) of four 3rd order spectral elements used for dispersion analysis.

numbers corresponding to the nodal points. Hence we have for the nodal points

$$
{}^{t}_{n_x h,\,n_y h}u = A_{k_h} e^{i(k_h n_x h\cos(\theta)+k_h n_y h\sin(\theta)-\omega_h t)} \tag{26}
$$

in which k_h is the computed wave number, A_{k_h} is a constant and ω_h is the computed frequency.

For our dispersion analysis we define the following functions based on Eq. (26)

$$
\begin{aligned}
f_1(n_x, n_y) &= 2\cos[k_h h(n_x\cos\theta + n_y\sin\theta)] \\
f_2(n_x, n_y) &= 2\cos[k_h h(n_x\cos\theta - n_y\sin\theta)] \\
f_3(n_y) &= 2\cos[k_h h(n_y\sin\theta)] \\
f_4(n_x) &= 2\cos[k_h h(n_x\cos\theta)]
\end{aligned} \tag{27}
$$

where, for example, $A_{k_h}e^{-i\omega_h t}f_1(0.5,\,1)$ denotes ${}_{0.5h,h}u + {}_{-0.5h,\,-h}u$.

4.1.1. 1st order traditional finite element

In this subsection, we consider first the traditional four-node finite element. The spatial dispersion analysis of Eq. (22) gives for the two-dimensional quadrilateral finite element for the **MÜ** term of the central node at ($x = 0, y = 0$) using Eq. (24) and a consistent mass matrix,

$$
\begin{aligned}
&\frac{h^2}{36}[16\,{}_{0,0}\ddot{u} + 4({}_{-h,0}\ddot{u} + {}_{h,0}\ddot{u} + {}_{0,-h}\ddot{u} + {}_{0,h}\ddot{u}) + ({}_{-h,-h}\ddot{u} + {}_{-h,h}\ddot{u} \\
&\quad + {}_{h,h}\ddot{u} + {}_{h,-h}\ddot{u})]
\end{aligned} \tag{28}
$$

and for the **KU** term

$$
\begin{aligned}
&\tfrac{c^2}{6}[16\,{}_{0,0}u - 2({}_{h,h}u + {}_{-h,h}u + {}_{h,-h}u + {}_{-h,-h}u) - 2({}_{-h,0}u + {}_{h,0}u) \\
&\qquad -2({}_{0,-h}u + {}_{0,h}u)]
\end{aligned} \tag{29}
$$

Using the relations in Eqs. (26)–(29) gives for a typical row in Eq. (23) corresponding to the center node of a patch (similar to that of Fig. 2)

$$
\begin{aligned}
&-\tfrac{h^2\omega_h^2 e^{-i\omega_h t}A_{k_h}}{36}[16 + f_1(1,\,1) + f_2(1,\,1) + 4(f_3(1) + f_4(1))] \\
&\tfrac{c^2 e^{-i\omega_h t}A_{k_h}}{6}[16 - 2(f_1(1,\,1) + f_2(1,\,1)) - 2(f_3(1) + f_4(1))] = 0
\end{aligned} \tag{30}
$$

In this analysis, a specific time integration scheme does not enter the above equation since we assume that a wave of the form in Eq. (26) is travelling through the mesh. Hence, the above relationship is valid for any time integration scheme used. However, we know that there are dispersion errors due to the spatial discretization and the time integration [17,29], hence we consider here only the errors due to the spatial discretization. Using $c_h = \frac{\omega_h}{k_h}$ we obtain

$$\frac{c_h}{c} = \frac{1}{k_h h}\left[\frac{96 - 12(f_1(1,1) + f_2(1,1)) - 12(f_3(1) + f_4(1))}{16 + f_1(1,1) + f_2(1,1) + 4f_3(1) + 4f_4(1)}\right]^{1/2} \tag{31}$$

where c_h denotes the numerical (or computed) wave velocity for the spatial discretization used. Discrepancies between the exact and numerical wave velocities are determined using Eq. (31) and are shown in Fig. 3a as a function of the computed wavelength λ_h (given by $2\pi/k_h$) and considering various values of the wave incident angle θ.

On the other hand, we arrive at the following dispersion relation when using the lumped mass matrix

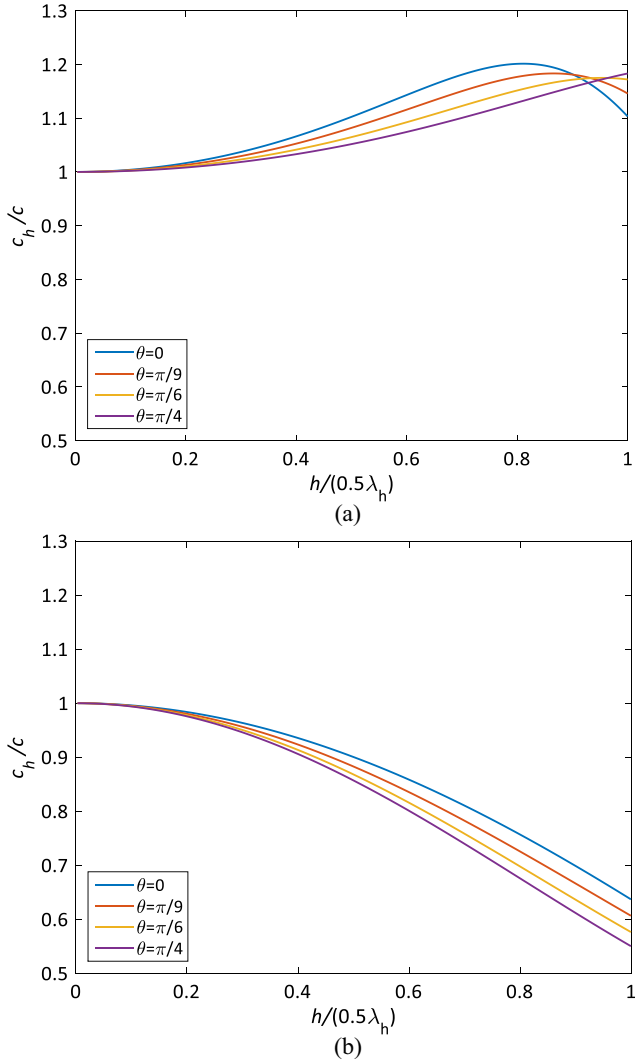

Fig. 3. Spatial dispersion of the 1st order quadrilateral finite element as a function of relative wavelength for various propagating angles: (a) using consistent mass matrix, and (b) using lumped mass matrix.

$$\frac{c_h}{c} = \frac{1}{k_h h}\left[\frac{8 - f_1(1,1) - f_2(1,1) - f_3(1) - f_4(1)}{3}\right]^{1/2} \tag{32}$$

Fig. 3b shows the results when a lumped mass matrix is used, showing that the spatial dispersion is quite large.

4.1.2. 3rd order spectral element

The **MÜ** term for the central node (using automatically a lumped mass matrix) is obtained as

$$\frac{h^2}{36}{}_{0,0}\ddot{u} \tag{33}$$

and the **KU** term for this node is

$$\begin{aligned} c^2\big[&\tfrac{26}{9}\,{}_{0,0}u - \tfrac{1}{36}\big({}_{-h,0}u + {}_{h,0}u + {}_{0,-h}u + {}_{0,h}u\big) \\ &+\big(\tfrac{5\sqrt{5}}{24} - \tfrac{25}{72}\big)\big({}_{-0.7236h,0}u + {}_{0.7236h,0}u + {}_{0,-0.7236h}u + {}_{0,0.7236h}u\big) \\ &-\big(\tfrac{5\sqrt{5}}{24} + \tfrac{25}{72}\big)\big({}_{-0.2764h,0}u + {}_{0.2764h,0}u + {}_{0,-0.2764h}u + {}_{0,0.2764h}u\big)\big] \end{aligned} \tag{34}$$

After rearranging Eqs. (33) and (34) and substituting $c_h = \frac{\omega_h}{k_h}$ we obtain

$$\begin{aligned} \tfrac{c_h}{c} = \tfrac{6}{k_h h}\Big[&\tfrac{26}{9} - \tfrac{1}{36}(f_3(1) + f_4(1)) + \big(\tfrac{5\sqrt{5}}{24} - \tfrac{25}{72}\big)(f_3(0.7236) + f_4(0.7236)) \\ &-\big(\tfrac{5\sqrt{5}}{24} + \tfrac{25}{72}\big)(f_3(0.2764) + f_4(0.2764))\Big]^{1/2} \end{aligned} \tag{35}$$

As seen in Eq. (35) and Fig. 2, only the central node and the nodes along the horizontal and vertical axes contribute to the expression. Fig. 4a shows the dispersion errors given by Eq. (35) for different values of propagating angles.

In the same way, we can evaluate the c_h/c curves for the 4th to the 8th order spectral elements. We give the details in Appendix B and show the results in Fig. 4. Note that the vertical axis scale in Fig. 4a is different from the scale in Fig. 3, and in Fig. 4b–f again a new scale is used. Fig. 4 shows that as the order of the element increases the dispersion error due to the spatial discretization decreases. Indeed, this error is very small for a high-order element, in particular for the elements of order equal to or greater than 5.

4.2. Establishing the CFL number

It is well established that, for an explicit time integration, the highest frequency of the frequencies of any element in the mesh can be used to establish a time step strictly equal to or smaller than the critical time step [12]. Hence, to establish a usable time step, strictly, we need to calculate the largest frequencies of the elements, or estimate a close upper bound. Accordingly, Table 1 gives the critical time steps for the 1st order finite element as well as various orders of spectral elements of size of $h \times h$ in the solution of the wave equation, Eq. (22). The values given are strict upper bounds to the highest frequency of the mesh using these elements and lead to the use of (see also Eq. (49))

$$\Delta t = \mathrm{CFL}^* \frac{h^*}{c} \tag{36a}$$

In practice, however, distorted elements are used and then either the exact highest element frequencies are calculated or a close upper bound is established [12]. This is the secure way to proceed so that the solution will not be unstable, but it may involve significant computations and the time step thus used may be smaller, and perhaps much smaller, than the actual critical time step of the mesh. It should be noted that values reported in Table 1 are rounded downwards to avoid using an unsuitable time step size.

Hence, it is also of interest to see whether we can derive an effective time step to use by considering the quadrilateral *spectral*

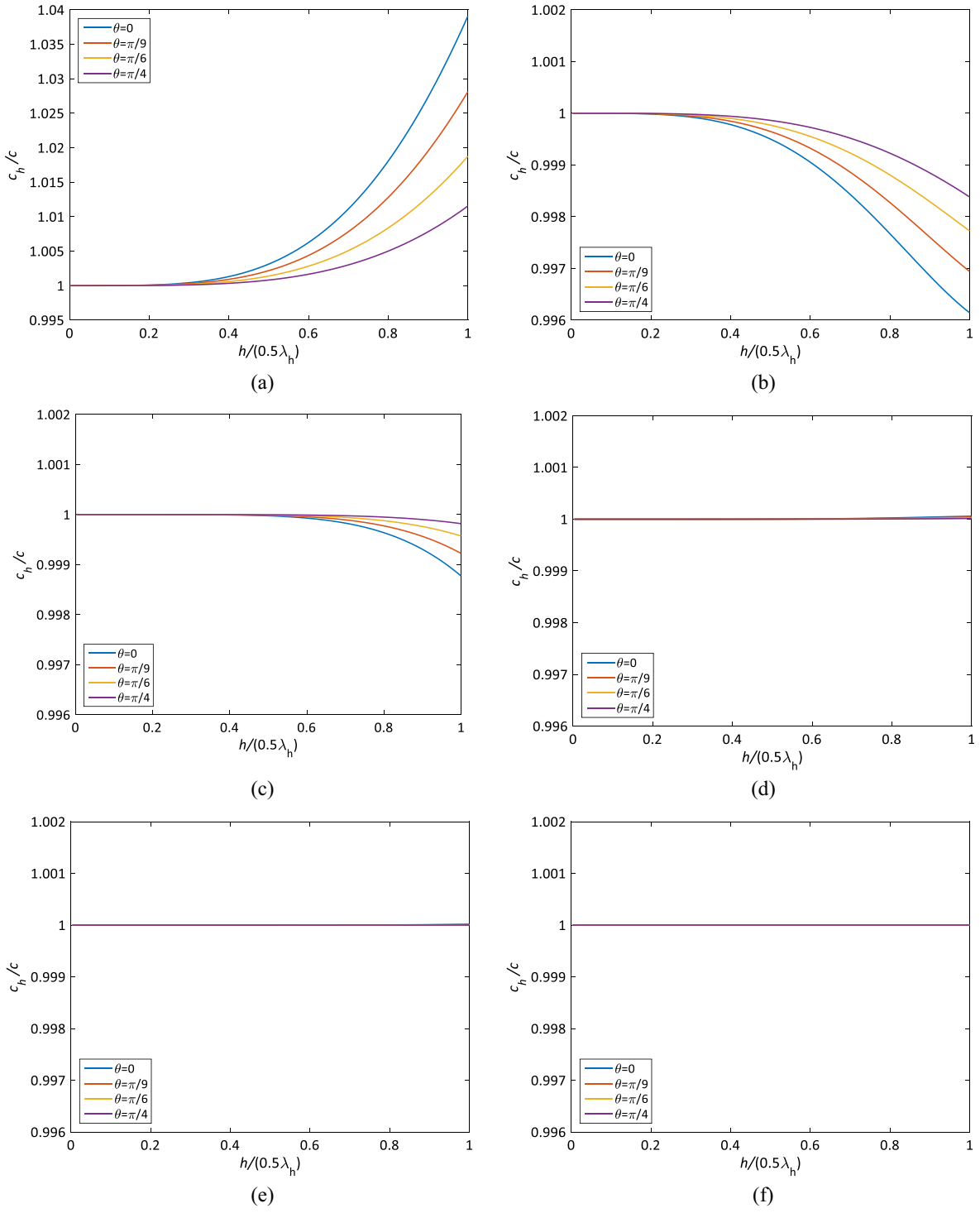

Fig. 4. Spatial dispersion of quadrilateral spectral elements of different orders as a function of relative wavelength for various propagating angles: (a) 3rd order, (b) 4th order, (c) 5th order, (d) 6th order, (e) 7th order, and (f) 8th order.

elements as higher-order elements of the quadrilateral *finite* element of first order. The CFL numbers for the classical 4-node finite element using the CDM and the NBM schemes are 1.0 and 1.85, respectively [15].

A simple way to proceed is to use the nodal spacing and wave velocity to establish a time step

$$\Delta t = \mathrm{CFL}\frac{d_{\min}}{c} \tag{36b}$$

where $d_{\min}$ is the "shortest distance" between any nodes in the mesh of elements. If multiple waves are seen in an analysis, c is the velocity of the fastest wave (usually the compression wave) in

Table 1
The critical time steps (rounded downwards to 4 digits) in terms of h^*/c computed for various quadrilateral elements of size $h \times h$; $h^* = h$ for the 4-node finite element using the lumped mass matrix.

Element type	Finite element		Spectral element					
	consistent mass matrix	lumped mass matrix						
Element order (n)	1	1	3	4	5	6	7	8
$\Delta t_{cr} = 2/\omega_n = h^*/c$	0.4082 h/c	h/c	0.1640 h/c	0.1044 h/c	0.0714 h/c	0.0516 h/c	0.0390 h/c	0.0304 h/c
$h^*/d_{\min}$	0.4082	1	0.1640/0.2764	0.1044/0.1727	0.0714/0.1175	0.0516/0.0849	0.0390/0.0641	0.0304/0.0501

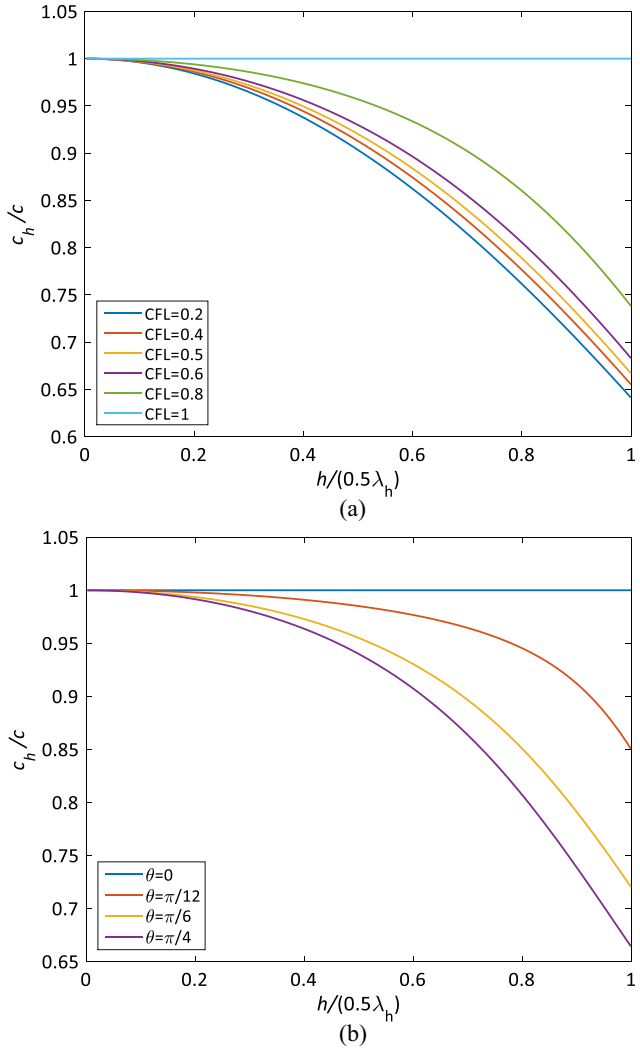

Fig. 5. Spatial-temporal dispersion of the central difference method using the 1st order quadrilateral finite element, with the lumped mass matrix, as a function of relative wavelength: (a) for various CFL numbers when $\theta = 0$, and (b) for various propagating angles when CFL = 1.

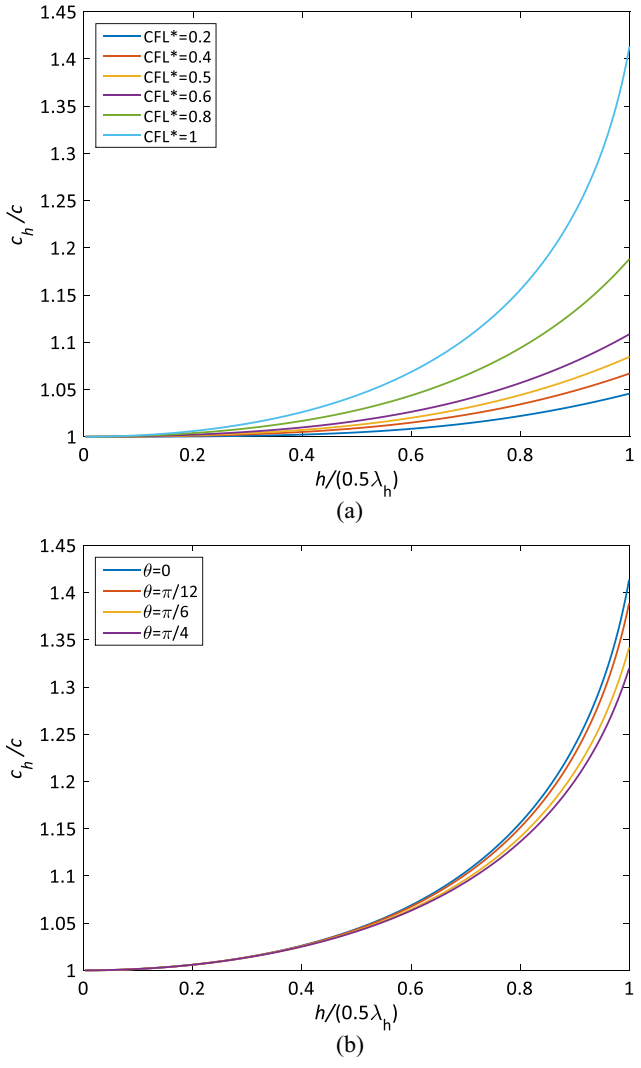

Fig. 6. Spatial-temporal dispersion using the central difference method and the 3rd order quadrilateral spectral element as a function of relative wavelength: (a) for various CFL* when $\theta = 0$, and (b) for various propagating angles when CFL* = 1.

the domain. However, for higher order elements, this formula may not give a good time step value for stability unless $d_{\min}$ is selected very conservatively. It is of interest to compare the value obtained for $d_{\min}$ from the nodal spacing of the elements with the values h^* calculated from the critical time steps, see Table 1.

4.3. Spatial-temporal dispersion of spectral elements

We next study the spatial-temporal dispersion using the CDM and the NBM. Since both space and time discretizations are carried out, we now use (instead of Eq. (26)) the following expression for solving Eq. (22)

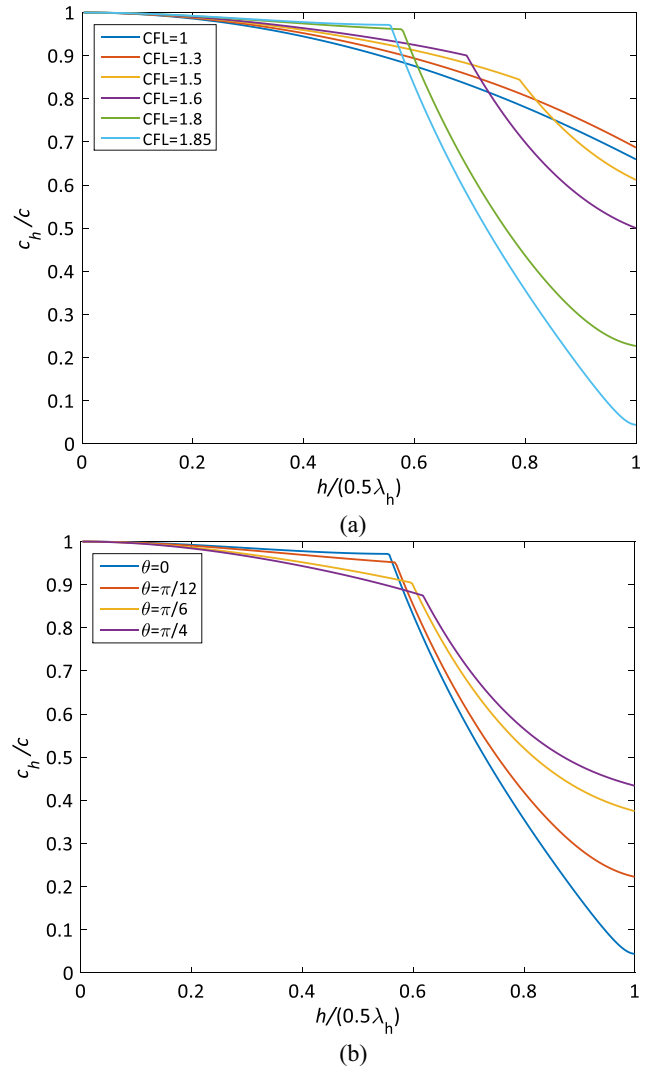

Fig. 7. Spatial-temporal dispersion of the Noh-Bathe method using the 1st order quadrilateral finite element with the lumped mass matrix as a function of relative wavelength; with $p = 0.54$: (a) for various CFL when $\theta = 0$, and (b) for various propagating angles when CFL = 1.85.

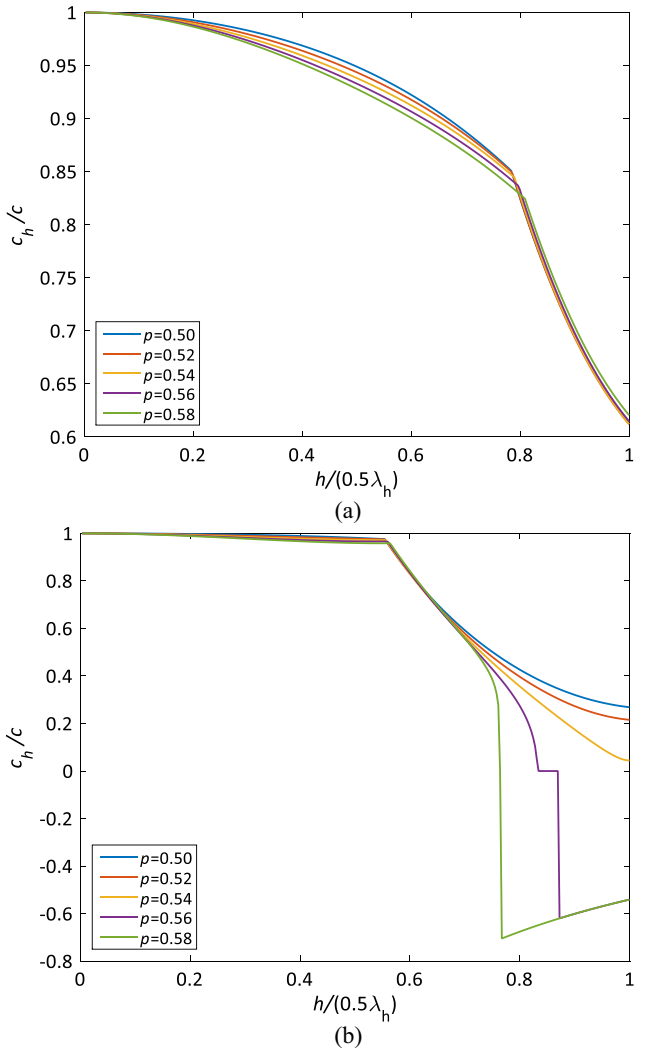

Fig. 8. Spatial-temporal dispersion of the Noh-Bathe method using the 1st order quadrilateral finite element with the lumped mass matrix as a function of relative wavelength for various values of p when $\theta = 0$: (a) CFL = 1.5, and (b) CFL = 1.85.

$$ {}^{n_t\Delta t}_{n_x h,\, n_y h}u = A_{k_h} e^{i(k_h n_x h\cos(\theta) + k_h n_y h\sin(\theta) - n_t \Delta t \omega_h)} \tag{37} $$

with $\omega_h = k_h c_h$ and n_t the time step counter.

Using $\mathrm{CFL} = \frac{c\Delta t}{h}$, we obtain

$$ {}^{n_t\Delta t}_{n_x h,\, n_y h}u = A_{k_h} e^{i(k_h n_x h\cos(\theta) + k_h n_y h\sin(\theta) - n_t k_h h \mathrm{CFL}(c_h/c))} \tag{38} $$

We recall that $n_x = n_y = 0$ corresponds to the position of the center node of the patch of the elements that we consider, see Fig. 2.

Of course, we can use the functions defined in Eq. (27) also in the spatial-temporal dispersion relations.

4.3.1. Central difference scheme

Using Eq. (5) with $\mathbf{C} = \mathbf{0}$ we have [12]

$$ {}^{t+\Delta t}\mathbf{U} + (-2\mathbf{I} + \frac{h^2 \mathrm{CFL}^2}{c^2}\mathbf{M}^{-1}\mathbf{K})\,{}^{t}\mathbf{U} + {}^{t-\Delta t}\mathbf{U} = \mathbf{0} \tag{39} $$

We use the term corresponding to the center node of the patch consisting of four elements to determine the numerical dispersion. Let g_1 be a function of the f_i functions in Eq. (27), corresponding to the $(h^2/c^2)(\mathbf{M}^{-1}\mathbf{K}\mathbf{U})$ term for the center node. Substituting Eq. (38) into Eq. (39) we obtain, using $n_t = 0$ for ease of arithmetic but without loss of generality,

$$ (A_{k_h} e^{i(-k_h h \mathrm{CFL}(c_h/c))} - 2A_{k_h} + A_{k_h} e^{i(k_h h \mathrm{CFL}(c_h/c))}) + \left(\frac{h^2 \mathrm{CFL}^2}{c^2}\frac{c^2 A_{k_h}}{h^2} g_1\right) = 0 \tag{40} $$

and hence

$$ \left(2A_{k_h}\cos\left(k_h h \mathrm{CFL}\frac{c_h}{c}\right) - 2A_{k_h}\right) + (A_{k_h}\mathrm{CFL}^2 g_1) = 0 \tag{41} $$

or

$$ 2\cos(k_h h \mathrm{CFL}\frac{c_h}{c}) + (2 + \mathrm{CFL}^2 g_1) = 0 \tag{42} $$

Thus, we arrive at the following form of dispersion relation – which is general for any element of any order

$$ \frac{c_h}{c} = \frac{1}{k_h h\,\mathrm{CFL}}\arccos\left(1 - \frac{\mathrm{CFL}^2}{2} g_1\right) \tag{43} $$

where g_1 depends on the spatial discretization expressed in terms of the functions defined in Eq. (27). The CDM is stable when the argument of $\arccos(.)$ is within $[-1, 1]$.

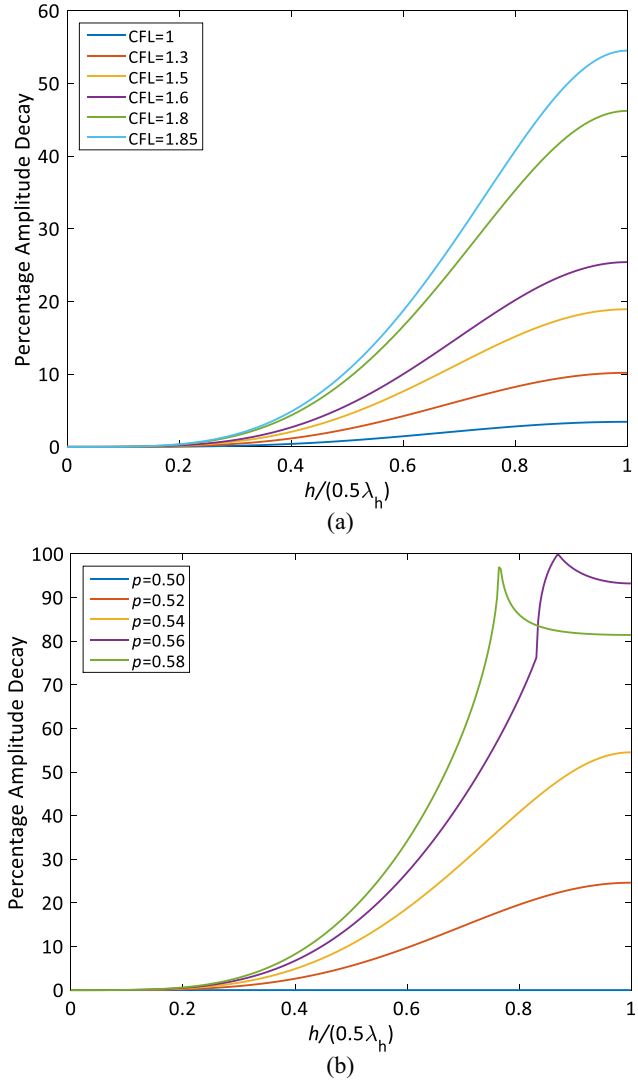

Fig. 9. Percentage amplitude decay of the Noh-Bathe method using the 1st order quadrilateral finite element with the lumped mass matrix as a function of relative wavelength; with $\theta = 0$: (a) for various CFL when $p = 0.54$, and (b) for various values p when CFL = 1.85.

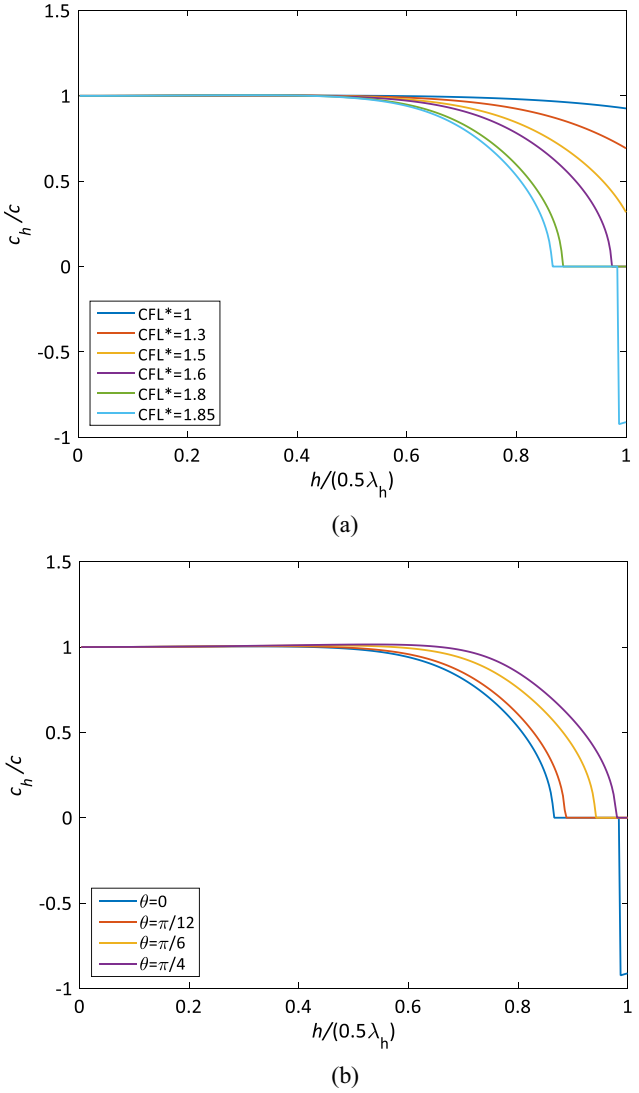

Fig. 10. Spatial-temporal dispersion of the Noh-Bathe method using the 3rd order quadrilateral spectral element as a function of relative wavelength; with $p = 0.54$: (a) for various CFL* when $\theta = 0$, and (b) for various propagating angles when CFL* = 1.85.

4.3.1.1. 1st order finite element. First, we assess the numerical dispersion using the 1st order finite element with the lumped mass matrix and the CDM. In this case, the $\mathbf{M}^{-1}\mathbf{KU}$ term for the central node is given by:

$$\frac{c^2}{3h^2}[8\ {}_{0,0}u - ({}_{h,h}u + {}_{-h,h}u + {}_{h,-h}u + {}_{-h,-h}u) - ({}_{-h,0}u + {}_{h,0}u) - ({}_{0,-h}u + {}_{0,h}u)] \tag{44}$$

where we only evaluate the spatial discretization because the time discretization is considered in Eq. (43) for which we now seek g_1. Combining Eqs. (27), (38) and (44) yields g_1

$$g_1 = \frac{1}{3}[8 - f_1(1,1) - f_2(1,1) - f_3(1) - f_4(1)] \tag{45}$$

Therefore, the dispersion relation Eq. (43) becomes

$$\frac{c_h}{c} = \frac{1}{k_h h \mathrm{CFL}}\arccos\left(1 - \frac{\mathrm{CFL}^2}{6}[8 - f_1(1,1) - f_2(1,1) - f_3(1) - f_4(1)]\right) \tag{46}$$

Fig. 5 shows that, as expected, we have no dispersion when CFL = 1 and $\theta = 0$. Of course, Eq. (46) degenerates to Eq. (32) in the limit as the CFL $\to 0$. Also, comparing the results given in Figs. 3b and 5, we see how the spatial and temporal dispersion errors "cancel each other out" when CFL = 1 and $\theta = 0$.

4.3.1.2. 3rd order spectral element. In this case the $\mathbf{M}^{-1}\mathbf{KU}$ term for the central node is

$$\begin{aligned}&\tfrac{c^2}{2h^2}[208\ {}_{0,0}u - 2({}_{-h,0}u + {}_{h,0}u + {}_{0,-h}u + {}_{0,h}u)\\ &+(15\sqrt{5}-25)({}_{-0.7236h,0}u + {}_{0.7236h,0}u + {}_{0,-0.7236h}u + {}_{0,0.7236h}u)\\ &-(15\sqrt{5}+25)({}_{-0.2764h,0}u + {}_{0.2764h,0}u + {}_{0,-0.2764h}u + {}_{0,0.2764h}u)]\end{aligned} \tag{47}$$

Hence, we have

$$\begin{aligned}g_1 = \frac{1}{2}[&208 - 2(f_3(1) + f_4(1)) + (15\sqrt{5}-25)(f_3(0.7236)\\ &+ f_4(0.7236)) - (15\sqrt{5}+25)(f_3(0.2764)\\ &+ f_4(0.2764))]\end{aligned} \tag{48}$$

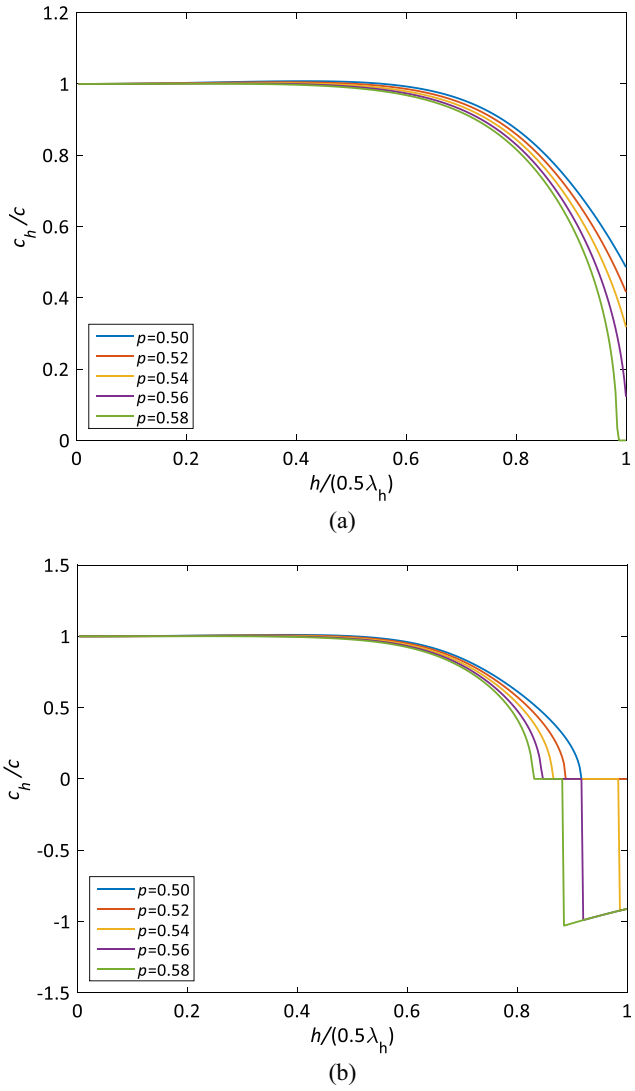

Fig. 11. Spatial-temporal dispersion of the Noh-Bathe method using the 3rd order quadrilateral spectral element as a function of relative wavelength for various values of p when $\theta = 0$: (a) CFL* = 1.5, and (b) CFL* = 1.85.

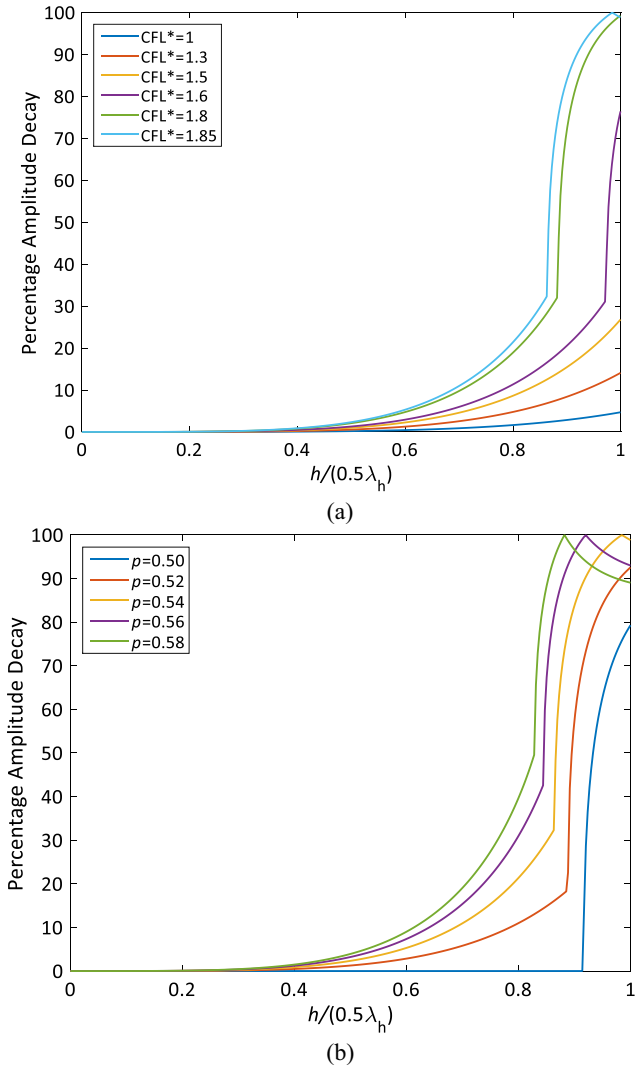

Fig. 12. Percentage amplitude decay of the Noh-Bathe method using the 3rd order quadrilateral spectral element as a function of relative wavelength; with $\theta = 0$: (a) for various CFL* when $p = 0.54$, and (b) for various values of p when CFL* = 1.85.

Let Δt_{cr} be h^*/c as reported in Table 1. Using $\text{CFL} = \frac{c\Delta t}{h}$ in Eq. (38) leads to a CFL number frequently used in spectral finite element solutions since $d_{\min}$ has already been used to calculate g_1. However, it is more strict to use h^* given in Table 1, and so we define $\text{CFL}^* = \frac{\text{CFL}}{h^*/d_{\min}} = \frac{d_{\min}}{h^*}\frac{c\Delta t}{h}$ corresponding to

$$\Delta t = \text{CFL}^* \frac{h^*}{c} \tag{49}$$

where h^* corresponds to an effective length. Clearly, the scale factor is $h^*/d_{\min}$. For the first order element $h^*/d_{\min} = 1$ but it decreases for higher order elements. In this study, Eq. (49) is employed for calculating the time step, and hence the scale factor is utilized.

For the 3rd order spectral element, the scale factor is equal to $h^*/d_{\min} = 0.1640/0.2764 = 0.5933$. Replacing CFL in Eq. (43) by $0.5933\ \text{CFL}^*$ and then using Eq. (48) give the dispersion relation

$$\frac{c_h}{c} = \frac{1}{0.5933 k_h h \text{CFL}^*}\arccos\Big(1 - \frac{0.5933^2 \text{CFL}^{*2}}{4}[208 - 2(f_3(1) + f_4(1)) + (15\sqrt{5} - 25)(f_3(0.7236) + f_4(0.7236)) - (15\sqrt{5} + 25)(f_3(0.2764) + f_4(0.2764))]\Big) \tag{50}$$

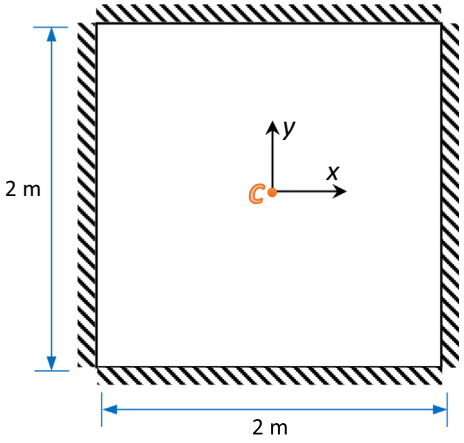

Fig. 13. Geometry of computational domain for two-dimensional scalar wave propagation in a pre-stressed membrane due to an excitation force applied at the center point C.

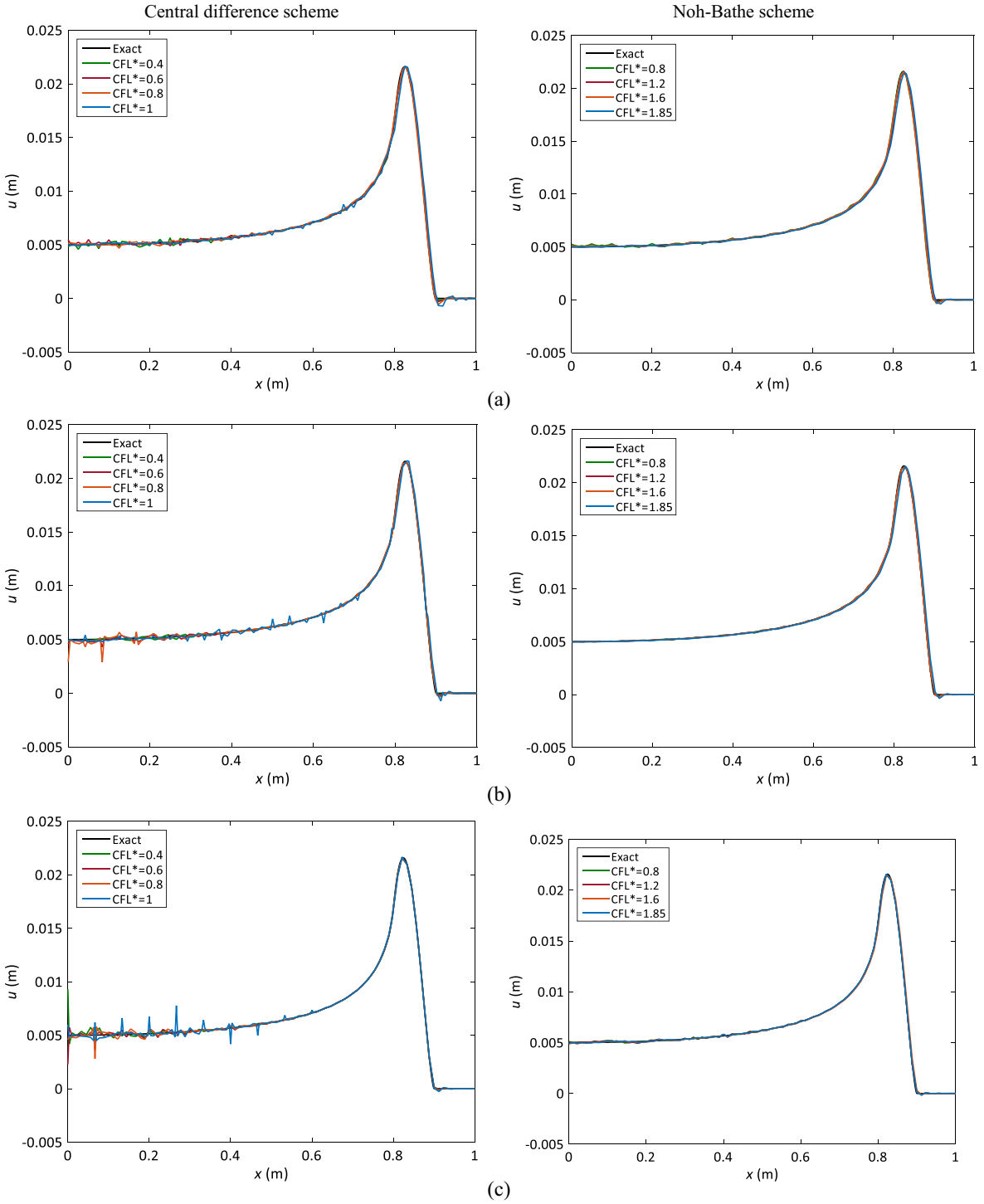

Fig. 14. Displacement variations along zero propagating angle using various CFL*, u (m) at time $t = 0.9$ s, using CDM (left) and NBM (right): (a) 3rd order spectral element with 80×80 element mesh, (b) 5th order spectral element with 48×48 element mesh, and (c) 8th order spectral element with 30×30 element mesh.

The result is shown in Fig. 6. We see that the maximum dispersion error is less than about 10 percent for the CFL* numbers smaller than 0.6.

4.3.2. Noh-Bathe scheme

Using the same procedure as for the CDM we obtain for the NBM

$$ {}^{t+\Delta t}\mathbf{U} + \left(-2\mathbf{I} + \frac{h^2\mathrm{CFL}^2}{c^2}\mathbf{M}^{-1}\mathbf{K} + \alpha_1 \frac{h^4\mathrm{CFL}^4}{c^4}\left(\mathbf{M}^{-1}\mathbf{K}\right)^2\right) {}^{t}\mathbf{U} + \left(\mathbf{I} + \beta_1 \frac{h^4\mathrm{CFL}^4}{c^4}\left(\mathbf{M}^{-1}\mathbf{K}\right)^2\right) {}^{t-\Delta t}\mathbf{U} = \mathbf{0} \tag{51} $$

with $\alpha_1 = \frac{1}{2}p^2(p-1)$ and $\beta_1 = -\frac{1}{2}p^3 + \frac{5}{4}p^2 - p + \frac{1}{4}$ being the numerical damping factors imposed by the NBM in order to suppress spurious high frequencies; p denotes the numerical damping ratio ranging from 0.5 to $2 - \sqrt{2}$.

Here we use the central node of a patch consisting of 16 elements to determine the numerical dispersion. All 16 elements in the patch (due to the bandwidth of $(\mathbf{M}^{-1}\mathbf{K})^2$) contribute to the term of the central node.

Utilizing Eq. (38) and Eq. (51) leads to

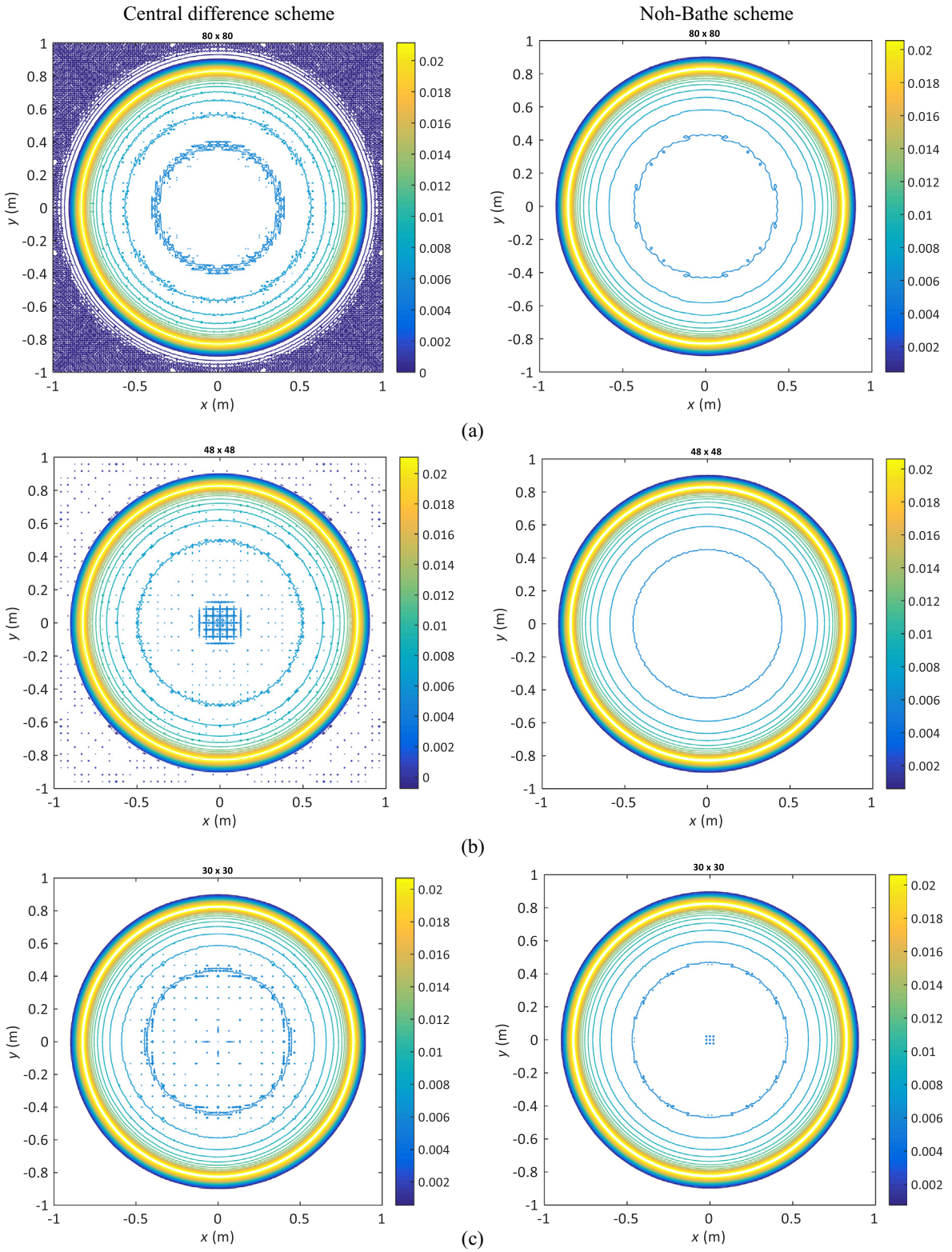

Fig. 15. Contour plots of displacement distributions, u (m) at $t = 0.9$ (s), using central difference scheme, CFL* = 1, (left) and Noh-Bathe scheme, CFL* = 1.85 (right): (a) 3rd order spectral element with 80 × 80 element mesh, (b) 5th order spectral element with 48 × 48 element mesh, and (c) 8th order spectral element with 30 × 30 element mesh.

$$A_{k_h}(e^{-i(k_h h\mathrm{CFL}(c_h/c))} + e^{i(k_h h\mathrm{CFL}(c_h/c))}) + \beta_1 \mathrm{CFL}^4 A_{k_h} e^{i(k_h h\mathrm{CFL}(c_h/c))} g_2 + (-2A_{k_h} + \mathrm{CFL}^2 A_{k_h} g_1 + \alpha_1 \mathrm{CFL}^4 A_{k_h} g_2) = 0 \quad (52)$$

for which c_h/c should be sought. Hence, the following form of dispersion relation is obtained – which is general for any element of any order

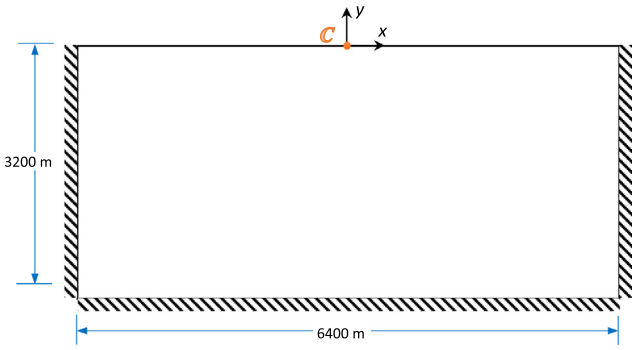

Fig. 16. Geometry of computational domain for two-dimensional wave propagations within a semi-infinite elastic medium (a Lamb problem) where the excitation force is applied at point C and two receivers are placed at $x = 640$ m and $x = 1280$ m on the surface boundary.

$$\frac{c_h}{c} = \frac{i}{k_h h \mathrm{CFL}} \ln\left(\frac{1}{2}\left[2 - \mathrm{CFL}^2 g_1 - \alpha_1 \mathrm{CFL}^4 g_2 - \sqrt{\left(-2 + \mathrm{CFL}^2 g_1 + \alpha_1 \mathrm{CFL}^4 g_2\right)^2 - 4(1 + \beta_1 \mathrm{CFL}^4 g_2)}\right]\right) \tag{53}$$

in which g_1 is a function corresponding to the $(h^2/c^2)(\mathbf{M}^{-1}\mathbf{KU})$ term for the central node; and g_2 is a function corresponding to the $(h^4/c^4)(\mathbf{M}^{-1}\mathbf{K})^2\mathbf{U}$ term for that node. Since the NBM is a dissipative scheme, c_h/c is a complex number: the real part gives the dispersion, and the imaginary part when negative gives the dissipation. We note that a non-monotonic behavior of the imaginary part (i.e., a sudden increase after a decrease) shows an instability.

The percentage amplitude decay [41] of the scheme can be determined by

$$AD = \left(1 - e^{\mathrm{Im}(\omega_h)\Delta t}\right) \times 100 \tag{54}$$

where $\omega_h = c_h k_h$ is equal to

Table 2
Normalized elapsed times to 1.0 and the corresponding CFL* for the analyses of the two Lamb problems, results are shown in Figs. 17–23.

Load function	Mesh	Element order (n)	CFL*		Normalized elapsed time	
			CDM	NBM	CDM	NBM
Case 1	400 × 200	3	1.2	2.2	1.2	1.2
	240 × 120	5	1.2	2.2	**1.0**	1.1
	150 × 75	8	1.2	2.2	1.7	1.7
Case 2	960 × 480	3	1.2	2.2	16.0	17.9
	576 × 288	5	1.2	2.2	14.3	15.8
	360 × 180	8	1.1	2.2	22.6	22.7

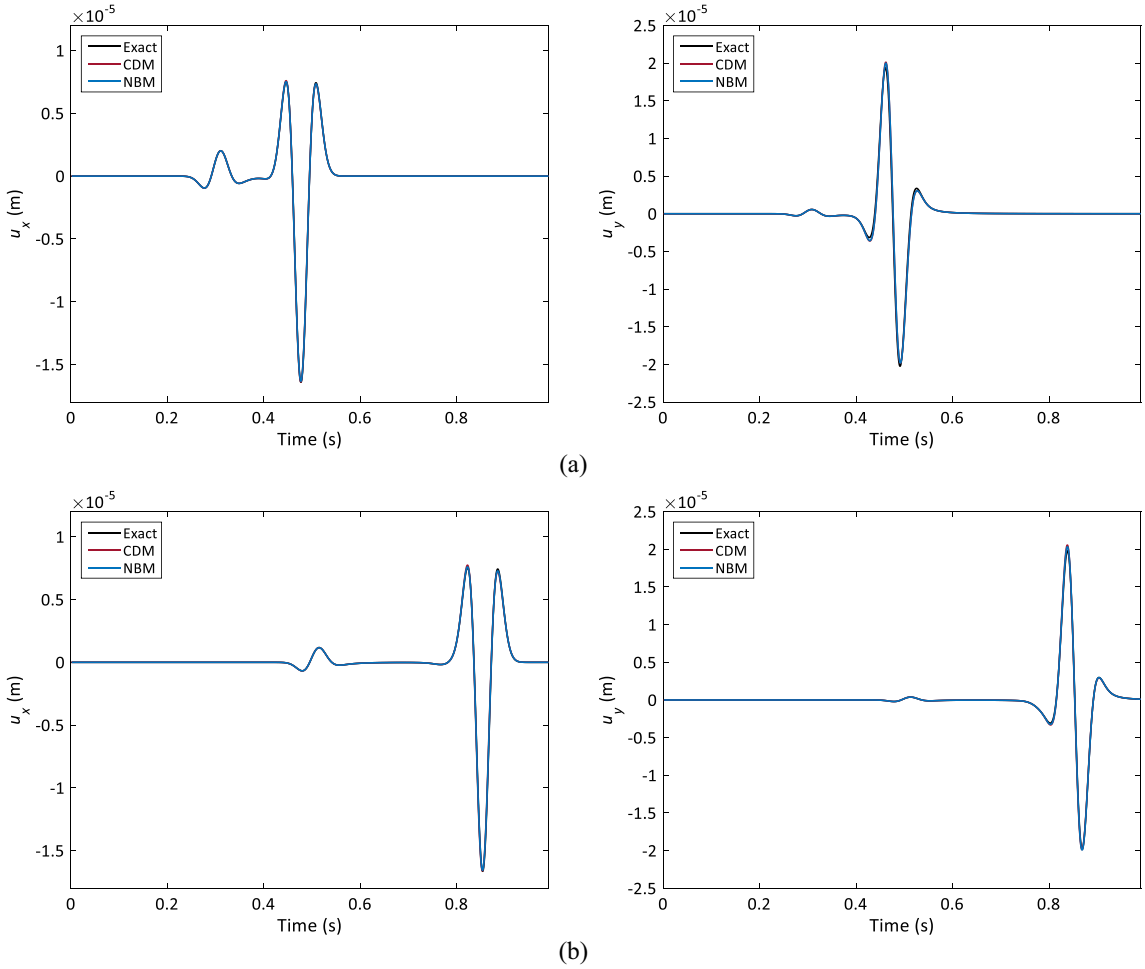

Fig. 17. Comparison of displacement histories obtained using 3rd order spectral element with 400 × 200 element mesh; Ricker wavelet excitation: (a) horizontal (left) and vertical (right) displacements at $x = 640$ m, and (b) horizontal (left) and vertical (right) displacements at $x = 1280$ m.

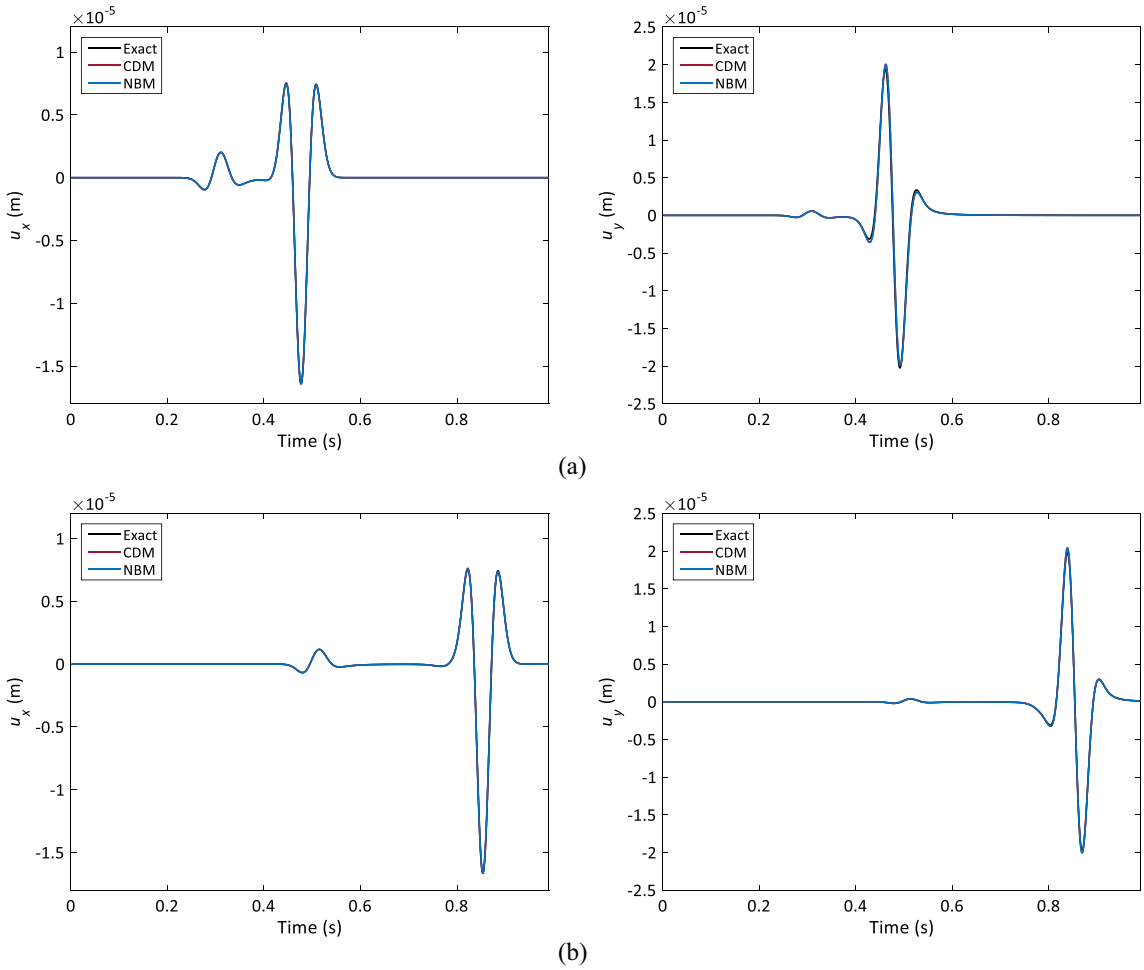

Fig. 18. Comparison of displacement histories obtained using 5th order spectral element with 240 × 120 element mesh; Ricker wavelet excitation: (a) horizontal (left) and vertical (right) displacements at x = 640 m, and (b) horizontal (left) and vertical (right) displacements at x = 1280 m.

$$\omega_h = \frac{i}{\Delta t}\ln\left(\frac{1}{2}\left[2 - \mathrm{CFL}^2 g_1 - \alpha_1 \mathrm{CFL}^4 g_2 - \sqrt{\left(-2 + \mathrm{CFL}^2 g_1 + \alpha_1 \mathrm{CFL}^4 g_2\right)^2 - 4(1 + \beta_1 \mathrm{CFL}^4 g_2)}\right]\right) \tag{55}$$

which is derived from Eq. (53). Of course, the amplitude decay calculated using Eq. (54) is due to both the spatial discretization and the time discretization.

4.3.2.1. 1st order finite element. We consider the use of the lumped mass matrix for which g_1 was previously obtained in Eq. (45). The $(\mathbf{M}^{-1}\mathbf{K})^2\mathbf{U}$ term for the central node is

$$\begin{aligned}\frac{c^4}{9h^4}[72\ {}_{0,0}u &- 14({}_{h,h}u + {}_{-h,h}u + {}_{h,-h}u + {}_{-h,-h}u)\\ &- 12({}_{-h,0}u + {}_{h,0}u) - 12({}_{0,-h}u + {}_{0,h}u)\\ &+ 3({}_{-2h,0}u + {}_{2h,0}u) + 3({}_{0,-2h}u + {}_{0,2h}u)\\ &+ 2({}_{2h,h}u + {}_{-2h,h}u + {}_{2h,-h}u + {}_{-2h,-h}u)\\ &+ 2({}_{h,2h}u + {}_{-h,2h}u + {}_{h,-2h}u + {}_{-h,-2h}u)\\ &+ ({}_{2h,2h}u + {}_{-2h,2h}u + {}_{2h,-2h}u + {}_{-2h,-2h}u)]\end{aligned} \tag{56}$$

Combining Eqs. (27), (38) and (56) leads to

$$\begin{aligned}g_2 = \frac{1}{9}[&72 - 14(f_1(1,1) + f_2(1,1)) - 12(f_3(1) + f_4(1))\\ &+ 3(f_3(2) + f_4(2)) + 2(f_1(2,1) + f_2(2,1) + f_1(1,2)\\ &+ f_2(1,2)) + f_1(2,2) + f_2(2,2)]\end{aligned} \tag{57}$$

Using Eqs. (45) and (57), the dispersion is calculated based upon Eq. (53). Fig. 7 shows some results for p = 0.54.

The choice of amount of numerical damping is an important issue when using a dissipative scheme. Fig. 8 shows the effect of p for two CFL numbers, CFL = 1.5 and 1.85. We see that the value p = 0.54 is a good value to use. Fig. 9 shows the percentage amplitude decay in terms of CFL numbers and various values of p. When p = 0.54, a larger CFL gives a larger amplitude decay, see Fig. 9a. For CFL = 1.85, as anticipated, the larger value of p leads to larger amplitude decay as shown in Fig. 9b. Thus, in order to have an efficient amplitude decay along with a small dispersion error, for this element, the use of CFL = 1.85 and p = 0.54 is a good choice, as recommended in Ref. [15].

4.3.2.2. 3rd order spectral element. For the 3rd order spectral element, g_1 was already determined in Eq. (48); now g_2 is obtained from the term $(\mathbf{M}^{-1}\mathbf{K})^2\mathbf{U}$ for the central node as follows:

$$\frac{c^4}{2h^4}[24440_{0,0}u + 4(_{h,h}u +_{-h,h} u +_{h,-h} u +_{-h,-h} u)$$
$$+(50-30\sqrt{5})(_{0.7236\,h,h}u +_{-0.7236\,h,h} u +_{0.7236\ h,-h} u +_{-0.7236\,h,-h} u$$
$$+_{h,0.7236\,h}u +_{-\,h,0.7236\,h} u +_{h,-0.7236\,h} u +_{-\,h,-0.7236\,h} u)$$
$$+(50+30\sqrt{5})(_{0.2764h,h}u +_{-0.2764h,h} u +_{0.2764h,-h} u +_{-0.2764\,h,-h} u$$
$$+_{h,0.2764h}u +_{-\,h,0.2764h} u +_{h,-0.2764\,h} u +_{-\,h,-0.2764h} u)$$
$$-500(_{0.2764h,0.7236h}u +_{-0.2764h,0.7236h} u$$
$$+_{0.2764h,-0.7236h}u +_{-0.2764\,h,-0.7236h} u$$
$$+_{0.7236h,0.2764h}u +_{-\,0.7236h,0.2764h} u$$
$$+_{0.7236h,-0.2764\,h}u +_{-\,0.7236h,-0.2764h} u)$$
$$+(1750-750\sqrt{5})(_{0.7236\,h,0.7236\,h}u$$
$$+_{-0.7236\,h,0.7236\,h}u +_{0.7236\,h,-0.7236\,h} u +_{-0.7236\,h,-0.7236\,h} u)$$
$$+(1750+750\sqrt{5})(_{0.2764\,h,0.2764\,h}u +_{-0.2764\,h,0.2764\,h} u$$
$$+_{0.2764\ h,-0.2764\ h}u +_{-0.2764\ h,-0.2764\ h} u)$$
$$+2(_{-2h,0}u +_{2h,0} u +_{0,-2h} u +_{0,2h} u)$$
$$+(25-15\sqrt{5})(_{-1.7236h,0}u +_{1.7236h,0} u +_{0,-1.7236h} u +_{0,1.7236h} u)$$
$$+(25+15\sqrt{5})(_{-1.2764h,0}u +_{1.2764h,0} u +_{0,-1.2764h} u +_{0,1.2764h} u)$$
$$-616(_{-h,0}u +_{h,0} u +_{0,-h} u +_{0,h} u)$$
$$+(-4125+2805\sqrt{5})(_{-0.7236h,0}u +_{0.7236h,0} u$$
$$+_{0,-0.7236h}u +_{0,0.7236h} u)$$
$$-(4125+2805\sqrt{5})(_{-0.2764h,0}u +_{0.2764h,0} u$$
$$+_{0,-0.2764h}u +_{0,0.2764h} u)] \tag{58}$$

Thus, we have

$$g_2 = \tfrac{1}{2}[24440 + 4(f_1(1,1) + f_2(1,1))$$
$$+(50-30\sqrt{5})(f_1(0.7236,1) + f_2(0.7236,1)$$
$$+f_1(1,0.7236) + f_2(1,0.7236))$$
$$+(50+30\sqrt{5})(f_1(0.2764,1) + f_2(0.2764,1)$$
$$+f_1(1,0.2764) + f_2(1,0.2764))$$
$$-500(f_1(0.2764,0.7236) + f_2(0.2764,0.7236)$$
$$+f_1(0.7236,0.2764) + f_2(0.7236,0.2764))$$
$$+(1750-750\sqrt{5})(f_1(0.7236,0.7236) + f_2(0.7236,0.7236))$$
$$+(1750+750\sqrt{5})(f_1(0.2764,0.2764) + f_2(0.2764,0.2764))$$
$$+2(f_3(2) + f_4(2)) + (25-15\sqrt{5})(f_3(1.7236) + f_4(1.7236))$$
$$+(25+15\sqrt{5})(f_3(1.2764) + f_4(1.2764)) - 616(f_3(1) + f_4(1))$$
$$+(-4125+2805\sqrt{5})(f_3(0.7236) + f_4(0.7236))$$
$$-(4125+2805\sqrt{5})(f_3(0.2764) + f_4(0.2764))] \tag{59}$$

Using the above procedure and replacing CFL by 0.5933 CFL*, the dispersion relation based on Eq. (53) is obtained. Some results are shown in Fig. 10 for $p = 0.54$. In comparison with Fig. 7, the dispersion error shown in Fig. 10 is considerably smaller. Furthermore, Fig. 10 shows that selecting CFL* = 1.85 can be unsafe for the 3rd order spectral element, while CFL* = 1.8 is a conservative choice.

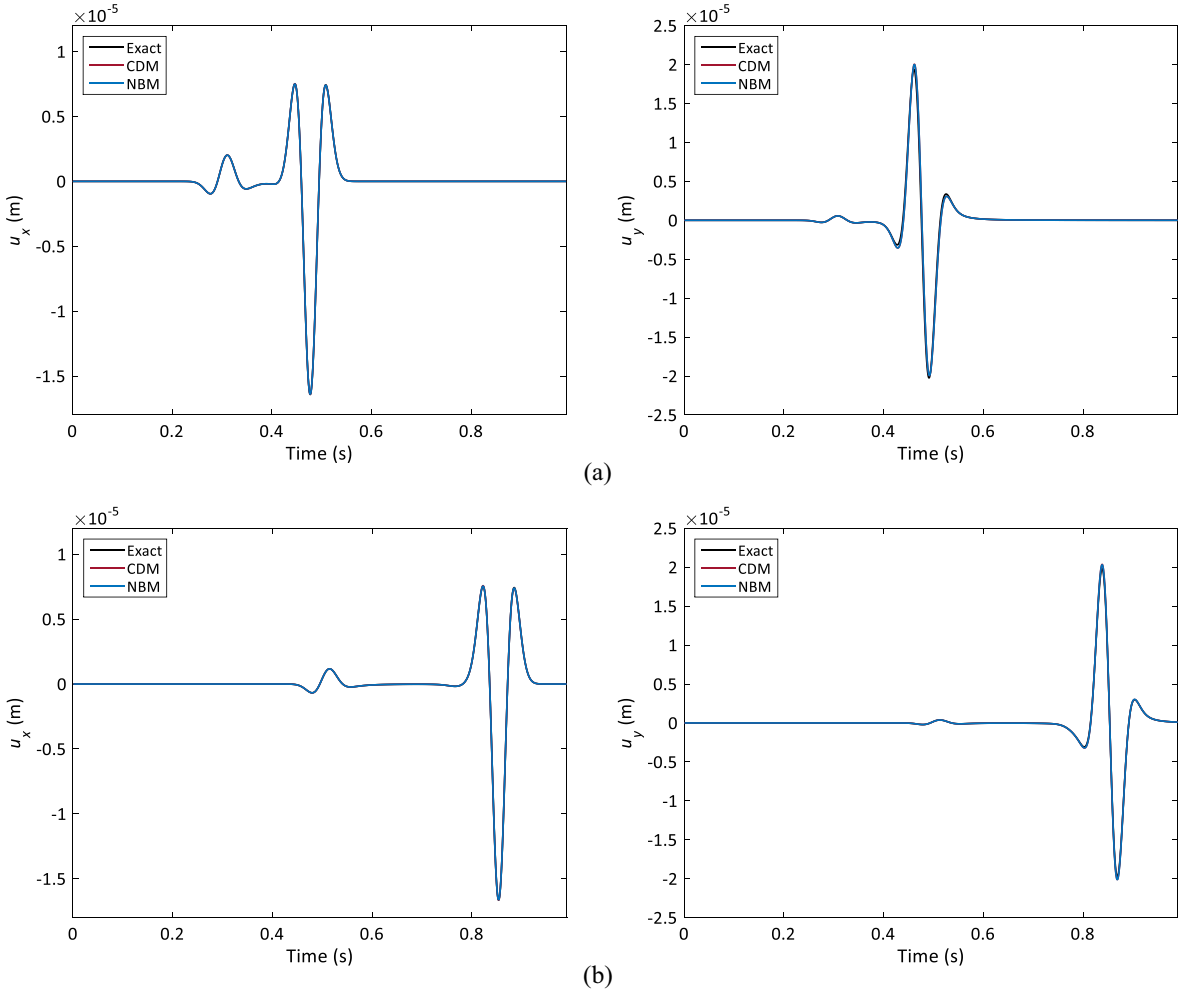

Fig. 19. Comparison of displacement histories obtained using 8th order spectral element with 150 × 75 element mesh; Ricker wavelet excitation: (a) horizontal (left) and vertical (right) displacements at $x = 640$ m, and (b) horizontal (left) and vertical (right) displacements at $x = 1280$ m.

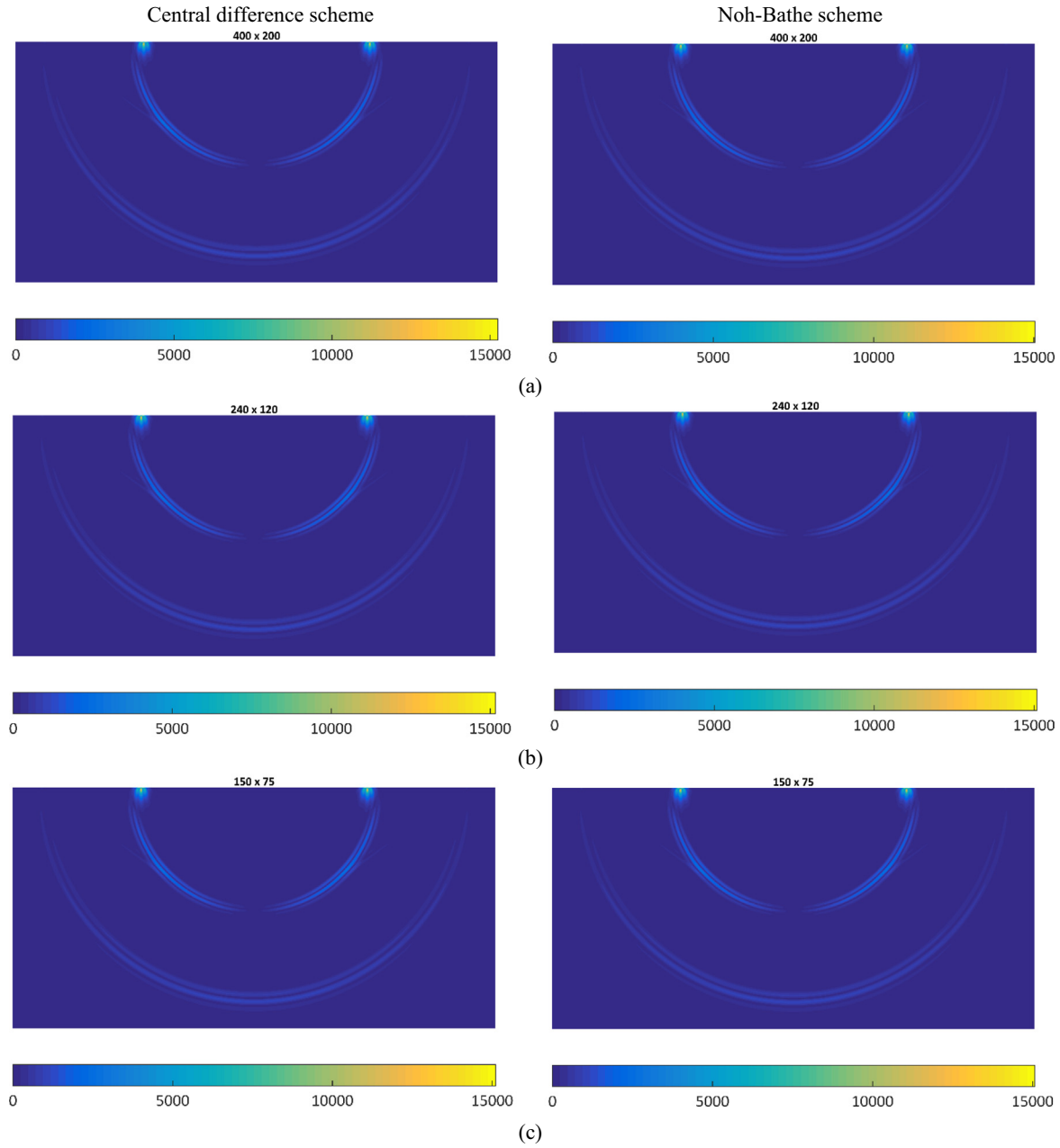

Fig. 20. Snapshots of von Mises stress at $t = 0.9828$ s, using central difference scheme (left) and Noh-Bathe scheme (right); Ricker wavelet excitation: (a) 3rd order spectral element using 400×200 element mesh, (b) 5th order spectral element using 240×120 element mesh, and (c) 8th order spectral element using 150×75 element mesh.

Figs. 11 and 12 illustrate that the effects of changing p are different from those seen when using the 1st order element. Significant sudden amplitude decays are seen at larger values of $h/0.5\lambda_h$ when using CFL* = 1.85, even with $p = 0.5$.

The derivation of the spatial-temporal dispersion for the spectral elements with an order higher than 3 can be pursued in the same manner as above.

5. Wave propagation solutions

In this section, we give solutions of wave propagation problems using the spectral elements and the CDM and the NBM. We use for the solutions, 3rd order, 5th order and 8th order spectral elements. Earlier investigations demonstrated that the spectral element with an order greater than 3 is useful for the analysis of wave propagations, while the highest order is usually selected to be 8 [4,25,42]. We use $p = 0.54$ for the NBM. First, we solve a two-dimensional transient scalar wave propagation problem and then we consider Lamb problems comprising different propagating waves in a semi-infinite elastic medium. In these examples, the solution time is such that the waves do not reach the truncated boundary of the model, hence we do not impose absorbing boundary conditions for suppressing artificially reflected waves. We performed the dynamic analyses using a PC with the Intel Core i7-4790 K CPU @ 4.00 GHz.

5.1. Two-dimensional scalar wave propagation in a pre-stressed membrane

Fig. 13 introduces the two-dimensional scalar wave propagation problem. A concentrated point excitation F_c at the center of

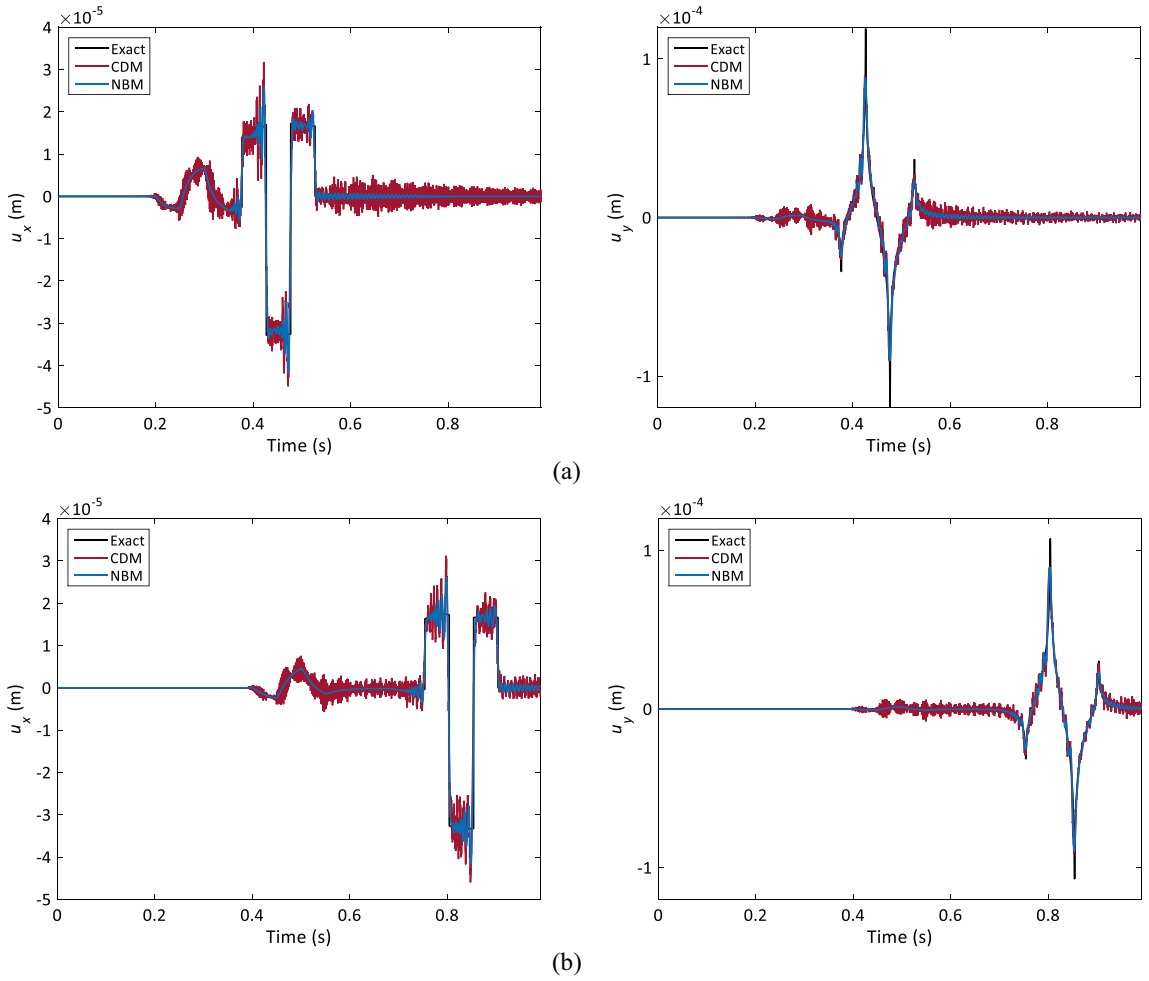

Fig. 21. Comparison of displacement histories obtained using 3rd order spectral element and 960 × 480 element mesh; excitation by step functions: (a) horizontal (left) and vertical (right) displacements at $x = 640$ m, and (b) horizontal (left) and vertical (right) displacements at $x = 1280$ m.

a pre-stressed membrane is considered [17]. The governing equation for the transverse displacement u is

$$\frac{\partial^2 u}{\partial x^2} + \frac{\partial^2 u}{\partial y^2} + F_c = \frac{1}{c^2}\frac{\partial^2 u}{\partial t^2} \tag{60}$$

with the wave velocity $c = 1$ m/s. We use the initial conditions

$$\begin{aligned} u(\mathbf{x} = \mathbf{0},\ t) &= 0 \text{ m}, \\ \dot{u}(\mathbf{x} = \mathbf{0},\ t) &= 0 \text{ m/s} \end{aligned} \tag{61}$$

and the force

$$F_c(\mathbf{x} = \mathbf{0},\ t) = 1.6 \times 10^2 t\,(0.1 - t)H(0.1 - t), \quad t > 0 \tag{62}$$

In Eq. (62), H is the Heaviside function. The computational domain is limited to $[-1, 1] \times [-1, 1]$ m, and the analytical solution of Eq. (60) is based on the Green's function and the convolution integral [43].

The meshes are 80 × 80 elements of order 3, 48 × 48 elements of order 5 and 30 × 30 elements of order 8 for which the number of DOFs are identical, each time for the complete membrane.

Fig. 14 shows displacement variations from the point of excitation by the force to the edge of the membrane. The numerical solutions are compared to the exact solution. Four CFL* numbers are considered for each element order. Overall, the NBM provides higher accuracy with diminishing spurious oscillations. Furthermore, snapshots of wave fronts at $t = 0.9$ s are shown in Fig. 15, demonstrating the reduction of spurious oscillations when using the NBM. Also, Fig. 15 shows that the solutions using the NBM are more accurate even for low order elements as they can capture the wave fronts better. As visible in Fig. 14 for the 8th order element, a higher order spectral element does not necessarily give a higher solution accuracy. This phenomenon can happen when a non-smooth function like Eq. (62) is considered. Using finer meshes, the spurious oscillations are reduced but then, of course, the cost of solution increases. Indeed, if the coarsest meshes using the CDM and NBM are employed to give (almost) no spurious oscillations, the solution using the NBM is significantly less costly.

5.2. Two-dimensional wave propagations in a semi-infinite elastic medium

We consider here the solution of wave propagations in a semi-infinite elastic medium, referred to as Lamb problems [15,17,44,45], see Fig. 16. Plane strain conditions are assumed for an isotropic semi-infinite elastic medium with mass density $\rho = 2200$ kg/m^3, P-wave velocity $c_p = 3200$ m/s and Poisson's ratio 0.25, giving the S-wave velocity $c_s = 1847.5$ m/s. The initial displacements and velocities are assumed to be zero and the computational domain is truncated to $[-3200, 3200] \times [-3200, 0]$ m. In the solutions, we use the maximum CFL* numbers for both the CDM and NBM, for which stability holds, as given in Table 2. These CFL* numbers are slightly larger than 1.0 and 1.85, for the CDM and NBM respectively, because we consider a plane strain elasticity

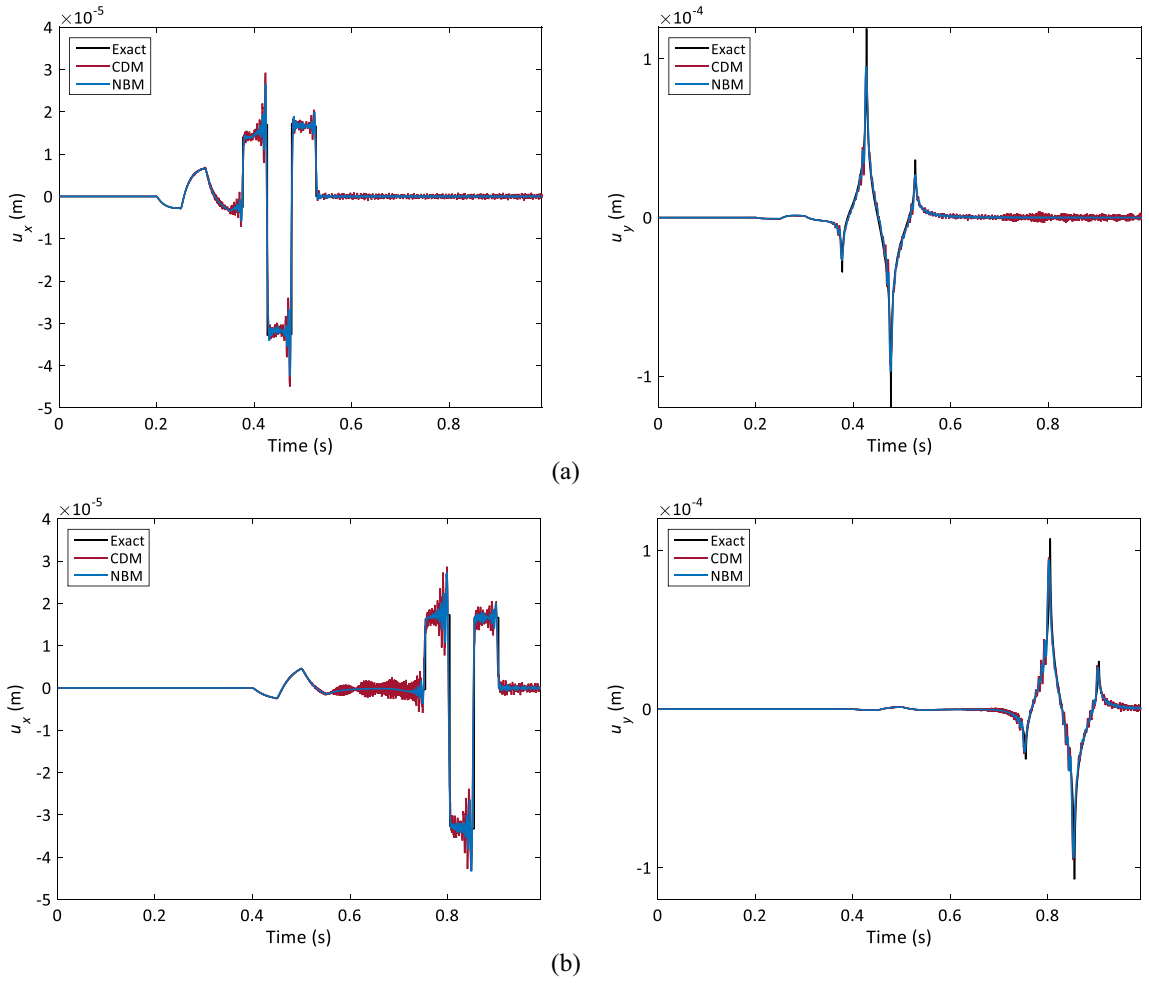

Fig. 22. Comparison of displacement histories obtained using 5th order spectral element with 576 × 288 element mesh; excitation by step functions: (a) horizontal (left) and vertical (right) displacements at $x = 640.5$ m, and (b) horizontal (left) and vertical (right) displacements at $x = 1281.7$ m.

problem. We established the CFL* in Table 2 using the fact that the critical wave velocity is larger and checked by numerical experimentation to identify when indeed the solutions become unstable. This illustrates that the results in Table 1 can also be used for other wave propagation problems to estimate an appropriate CFL*.

We consider separately two concentrated load cases consisting of a Ricker wavelet excitation and an excitation by a sum of step functions. The analytical solutions are based on the Green's function as per Ref. [44] and the convolution integral.

The concentrated Ricker force is located at the center of the free surface

$$F_c = -10^6(1 - 2\pi^2\hat{f}^2(t - t_0)^2)\exp(-\pi^2\hat{f}^2(t - t_0)^2), \quad t > 0 \qquad (63)$$

where $\hat{f}$ and t_0 are taken as 12.5 Hz and 0.1 s, respectively. We use three meshes of different spectral element orders with identical number of DOFs: a mesh of 400 × 200 elements of element order 3, a mesh of 240 × 120 elements of order 5 and a mesh of 150 × 75 elements of order 8. Figs. 17–19 show the predicted horizontal and vertical surface displacements at $x = 640$ m and $x = 1280$ m, where the receivers are located, in comparison with the analytical solutions. All predicted solutions using the CDM and NBM are very accurate. Fig. 20 depicts snapshots of the predicted von Mises stress at $t = 0.9828$ s. Hence in this analysis, the meshes and time steps used are appropriate for an accurate numerical solution.

A more difficult problem to solve accurately is obtained when the following concentrated force is applied

$$F_c = 10^6[H(0.15 - t) - 3H(0.1 - t) + 3H(0.05 - t)], \quad t > 0 \qquad (64)$$

which requires much finer meshes to achieve a reasonably accurate solution. We now use a mesh of 960 × 480 elements of order 3, a mesh of 576 × 288 elements of order 5 and a mesh of 360 × 180 elements of order 8, so that we have in all solutions 4,151,521 nodes for the complete domain considered (we do not use symmetry). As in the previous case, we use the element-by-element assemblage to calculate the required vectors for both integration schemes. The predicted horizontal and vertical surface displacements at the positions of the receivers (i.e., at $x = 640$ m and $x = 1280$ m) are shown in Figs. 21–23 with the analytical solutions. The response predictions are not very accurate but reasonable and the solutions using the NBM show less oscillations. The CFL* used corresponding to the results shown in Figs. 21–23 are listed in Table 2. In addition, we give in Figs. 24 and 25 the solutions using the CDM with CFL* = 1.2 and 1.0. We see that although the CDM can be used with CFL* = 1.2 (like for the other elements), the response prediction is very inaccurate. Here we have a case in which the solution does not "blow up" showing instability when using the CDM but simply is very inaccurate – this can be of particular concern in the solution of practical engineering problems and is not found when using the NBM. In comparing the solutions obtained using the CDM and NBM, we see that for this problem, using the NBM gives a reasonable

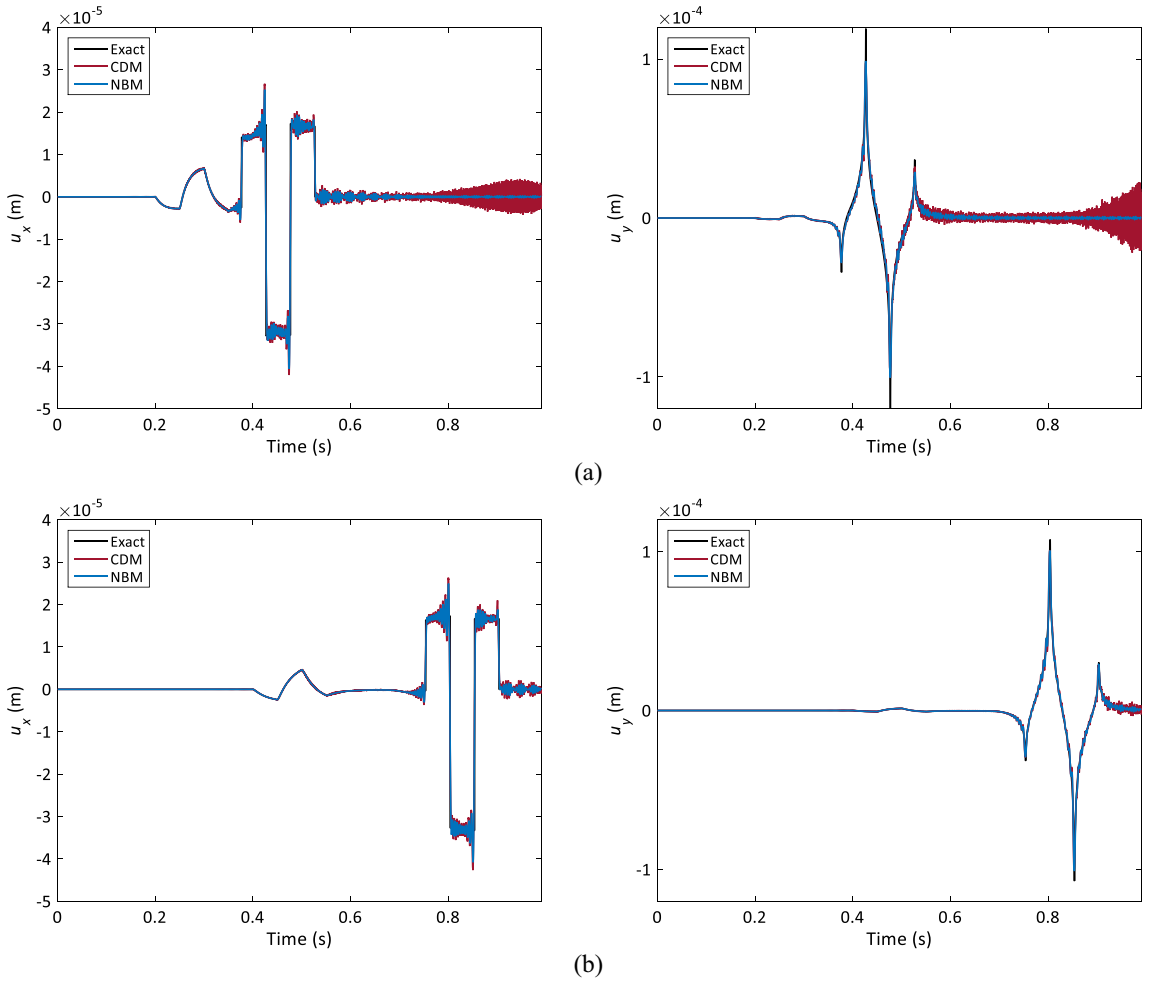

Fig. 23. Comparison of displacement histories obtained using 8th order spectral element with 360 × 180 element mesh; excitation by step functions: (a) horizontal (left) and vertical (right) displacements at x = 640 m, and (b) horizontal (left) and vertical (right) displacements at x = 1280 m.

response prediction even when employing more than two times larger a CFL*, that is CFL* = 2.2.

These solutions show that when using spectral elements in the analyses of wave propagations, the differences in accuracy obtained with the CDM and NBM, can be more significant when using lower order elements and/or when the loading forces high frequency transient excitations. Table 2 also lists normalized computational times for each analysis performed. We see that the computational times using the NBM are near to those using the CDM, while providing better accuracy.

6. Concluding remarks

We focused in this research on the performance of the Noh-Bathe explicit time integration scheme when compared with the central difference scheme and used in the analysis of wave propagations with spectral finite elements. We calculated spatial dispersion relations for spectral elements, and also derived spatial-temporal dispersion relations for both the CDM and NBM which can be employed for different elements.

Although the NBM requires the "internal" calculations in a time step due to a sub-step, the computational effort is near the effort employed for the CDM due to the use of a 1.85 to 2 times larger CFL* numbers. An advantage is that the use of the NBM can provide, using the same mesh, higher accuracy with lower spurious oscillations. However, since the use of spectral elements can significantly reduce the spatial numerical dispersion, the solution difference between using the two schemes may in some analyses not be significant. The improved accuracy and elimination of spurious oscillations using the NBM are visible for every element order when a complex transient excitation is imposed, in which a large number of high frequency vibration modes contribute to the response. But here we might note that for the solution of the Lamb problem with the step loadings, the overlapping finite elements used with the implicit Bathe scheme are quite effective [45].

Another advantage in the use of the NBM scheme is that a banded damping matrix can directly be included without a very large increase in the solution cost. Hence Rayleigh damping including the stiffness matrix term can be used and absorbing boundary conditions providing a bandwidth can be included.

Although we considered in this paper the solution of model problems, the theoretical derivations and insights obtained are valuable for the solution of general transient wave propagation problems.

Declaration of Competing Interest

The authors declare that they have no known competing financial interests or personal relationships that could have appeared to influence the work reported in this paper.

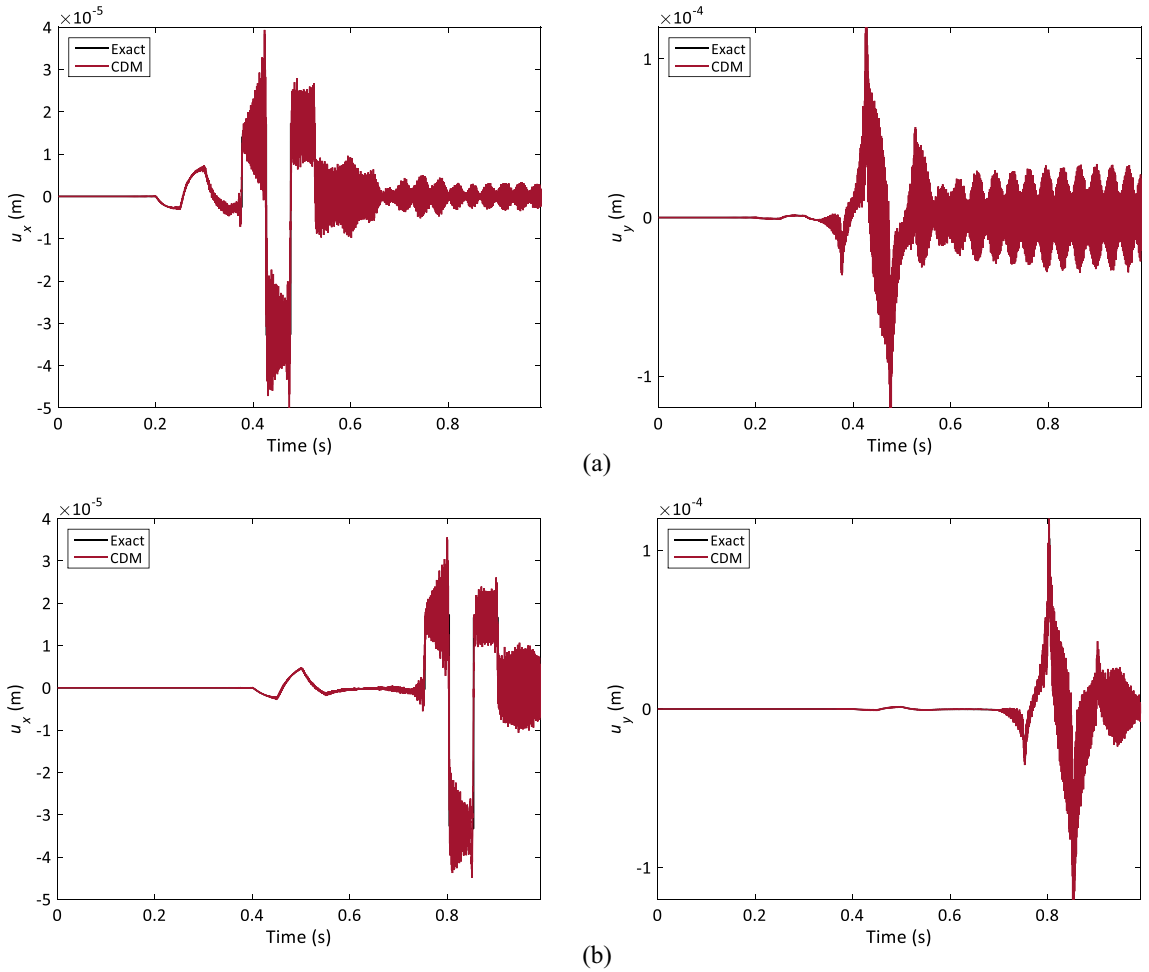

Fig. 24. Displacement histories obtained using 8th order spectral element with 360 × 180 element mesh; CFL* = 1.2; excitation by step functions: (a) horizontal (left) and vertical (right) displacements at $x = 640$ m, and (b) horizontal (left) and vertical (right) displacements at $x = 1280$ m.

Appendix A

We present here the mass and stiffness matrices of square quadrilateral elements used in the paper; h and c are the element "length" and wave velocity, respectively. For the 1st order quadrilateral finite element, the mass and stiffness matrices are given by:

$$\mathbf{M}^{(m)} = \frac{h^2}{36}\begin{bmatrix} 4 & 2 & 2 & 1 \\ & 4 & 1 & 2 \\ & & 4 & 2 \\ sym. & & & 4 \end{bmatrix} \tag{A.1}$$

$$\mathbf{K}^{(m)} = \frac{c^2}{6}\begin{bmatrix} 4 & -1 & -1 & -2 \\ & 4 & -2 & -1 \\ & & 4 & -1 \\ sym. & & & 4 \end{bmatrix} \tag{A.2}$$

For the 3rd order quadrilateral spectral element shown in Fig. 1, the mass and stiffness matrices are given by:

$$diag(\mathbf{M}^{(m)}) = \frac{h^2}{144}[1,\ 5,\ 5,\ 1,\ 5,\ 25,\ 25,\ 5,\ 5,\ 25,\ 25,\ 5,\ 1,\ 5,\ 5,\ 1] \tag{A.3}$$

where $diag(.)$ means that the mass matrix is diagonal and only the diagonal elements are listed, and

$$\mathbf{K}^{(m)} = c^2\begin{bmatrix} \mathbf{k}_1 & \mathbf{k}_5 & \mathbf{k}_3 & \mathbf{k}_4 \\ \mathbf{k}_5 & \mathbf{k}_2 & 25\mathbf{k}_4 & \mathbf{k}_3 \\ \mathbf{k}_3 & 25\mathbf{k}_4 & \mathbf{k}_2 & \mathbf{k}_5 \\ \mathbf{k}_4 & \mathbf{k}_3 & \mathbf{k}_5 & \mathbf{k}_1 \end{bmatrix} \tag{A.4}$$

in which the block matrices are

$$\mathbf{k}_1 = \begin{bmatrix} 13/18 & -a-b & a-b & -1/72 \\ -a-b & 5/2 & -25/72 & a-b \\ a-b & -25/72 & 5/2 & -a-b \\ -1/72 & a-b & -a-b & 13/18 \end{bmatrix} \tag{A.5}$$

$$\mathbf{k}_2 = \begin{bmatrix} 5/2 & -5a-5b & 5a-5b & -5/72 \\ -5a-5b & 125/18 & -125/72 & 5a-5b \\ 5a-5b & -125/72 & 125/18 & -5a-5b \\ -5/72 & 5a-5b & -5a-5b & 5/2 \end{bmatrix} \tag{A.6}$$

$$\mathbf{k}_3 = \begin{bmatrix} a-b & 0 & 0 & 0 \\ 0 & 5a-5b & 0 & 0 \\ 0 & 0 & 5a-5b & 0 \\ 0 & 0 & 0 & a-b \end{bmatrix} \tag{A.7}$$

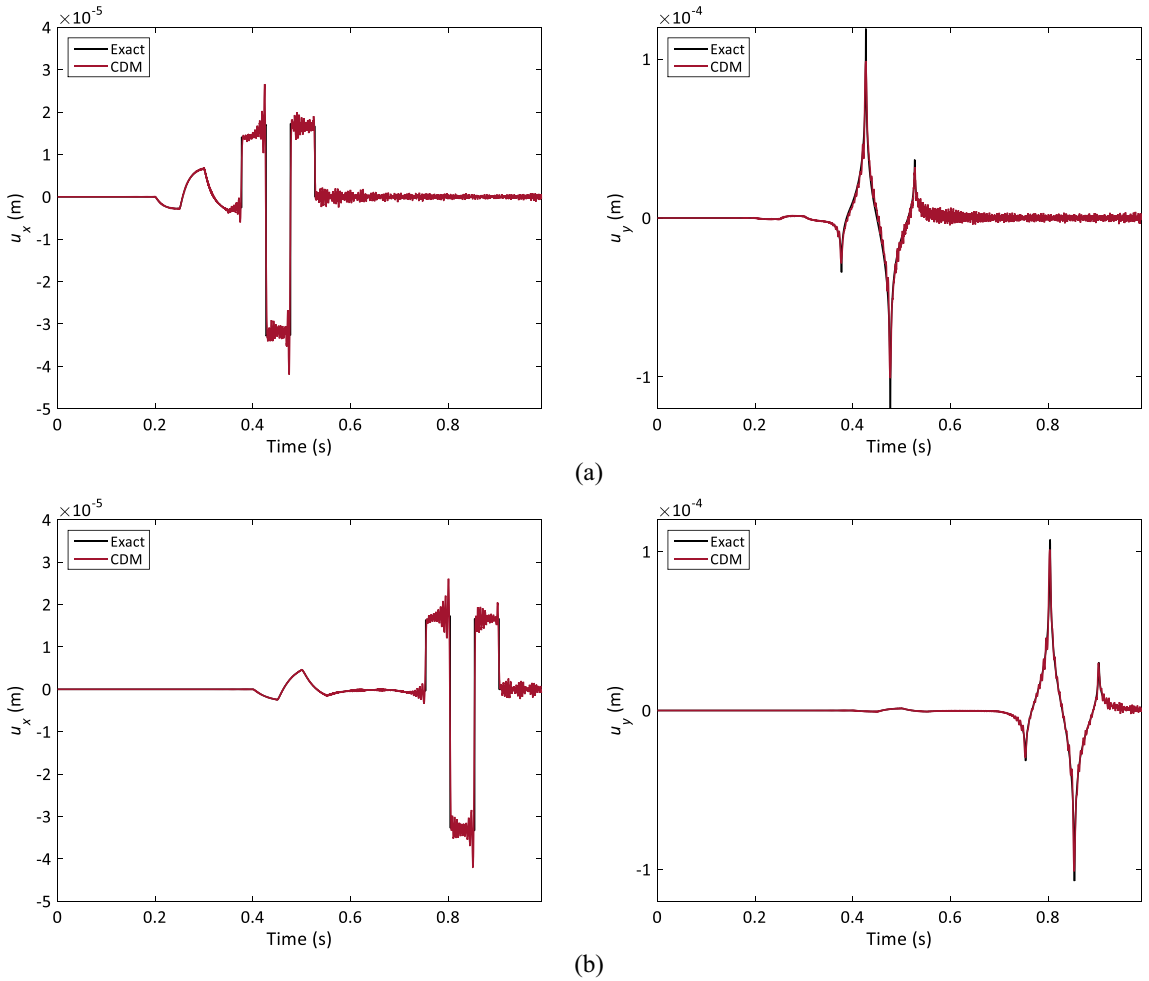

Fig. 25. Displacement histories obtained using 8th order spectral element with 360 × 180 element mesh; CFL* = 1; excitation by step functions: (a) horizontal (left) and vertical (right) displacements at x = 640 m, and (b) horizontal (left) and vertical (right) displacements at x = 1280 m.

$$\mathbf{k}_4 = \begin{bmatrix} -1/72 & 0 & 0 & 0 \\ 0 & -5/72 & 0 & 0 \\ 0 & 0 & -5/72 & 0 \\ 0 & 0 & 0 & -1/72 \end{bmatrix} \tag{A.8}$$

$$\mathbf{k}_5 = \begin{bmatrix} -a-b & 0 & 0 & 0 \\ 0 & -5a-5b & 0 & 0 \\ 0 & 0 & -5a-5b & 0 \\ 0 & 0 & 0 & -a-b \end{bmatrix} \tag{A.9}$$

with $a = 5\sqrt{5}/48$ and $b = 25/144$.

Appendix B

4th order spectral element:

The **MÜ** term for the central node at (x = 0, y = 0) is expressed as

$$0.01\, h^2{}_{0,0}\ddot{u} \tag{B.1}$$

and the **KU** term for this node is

$$\begin{aligned} &c^2[2.8_{x,y}u + 0.01(_{-h,\,0}u +_{h,\,0} u +_{0,\,-h} u +_{0,\,h} u) \\ &-0.0341(_{-0.8273h,\,0}u +_{0.8273h,\,0} u +_{0,\,-0.8273h} u +_{0,\,0.8273h} u) \\ &+0.1067(_{-0.5h,\,0}u +_{0.5h,\,0} u +_{0,\,-0.5h} u +_{0,\,0.5h} u) \\ &- 0.7826(_{-0.1727h,\,0}u +_{0.1727h,\,0} u +_{0,\,-0.1727h} u +_{0,\,0.1727h} u)] \end{aligned} \tag{B.2}$$

thus, we have

$$\begin{aligned} \tfrac{c_h}{c} = \tfrac{10}{k_h h}[&2.8 + 0.01(f_3(1)+f_4(1)) - 0.3041(f_3(0.8273)+f_4(0.8273)) \\ &+0.1067(f_3(0.5)+f_4(0.5)) - 0.7826(f_3(0.1727)+f_4(0.1727))]^{1/2} \end{aligned} \tag{B.3}$$

Fig. 4b shows the dispersion curves obtained using Eq. (B.3) for different values of propagating angles.

5th order spectral element:

The **MÜ** term gives

$$0.0044 h^2_{0,\,0}\ddot{u} \tag{B.4}$$

while the **KU** term is expanded as

$$\begin{aligned} &c^2[2.7555_{0,\,0}u - 0.0044(_{-h,\,0}u +_{h,\,0} u +_{0,\,-h} u +_{0,\,h} u) \\ &+0.0136(_{-0.8825h,\,0}u +_{0.8825h,\,0} u +_{0,\,-0.8825h} u +_{0,\,0.8825h} u) \\ &- 0.0310(_{-0.6426h,\,0}u +_{0.6426h,\,0} u +_{0,\,-0.6426h} u +_{0,\,0.6426h} u) \\ &+0.1004(_{-0.3574h,\,0}u +_{0.3574h,\,0} u +_{0,\,-0.3574h} u +_{0,\,0.3574h} u) \\ &- 0.7674(_{-0.1175h,\,0}u +_{0.1175h,\,0} u +_{0,\,-0.1175h} u +_{0,\,0.1175h} u)] \end{aligned} \tag{B.5}$$

Hence, we reach

$$\frac{c_h}{c} = \frac{1}{\sqrt{0.0044 k_h h}}[2.7555 - 0.0044(f_3(1) + f_4(1)) + 0.0136(f_3(0.8825) + f_4(0.8825)) - 0.0310(f_3(0.6426) + f_4(0.6426)) + 0.1004(f_3(0.3574) + f_4(0.3574)) - 0.7674(f_3(0.1175) + f_4(0.1175))]^{1/2} \quad \text{(B.6)}$$

which is used in Fig. 4c.

6th order spectral element:

The **MÜ** term for the central node is expanded as

$$0.0023\ h^2_{0,0}\ddot{u} \quad \text{(B.7)}$$

and the **KU** term for the central node is formulated as

$$c^2[2.7302_{0,0}u + 0.0023(_{-h,0}u +_{h,0} u +_{0,-h} u +_{0,h} u) - 0.0065(_{-0.9151h,0}u +_{0.9151h,0} u +_{0,-0.9151h} u +_{0,0.9151h} u) + 0.0127(_{-0.7344h,0}u +_{0.7344h,0} u +_{0,-0.7344h} u +_{0,0.7344h} u) - 0.0290(_{-0.5h,0}u +_{0.5h,0} u +_{0,-0.5h} u +_{0,0.5h} u) + 0.0968(_{-0.2656h,0}u +_{0.2656h,0} u +_{0,-0.2656h} u +_{0,0.2656h} u) - 0.7587(_{-0.0849h,0}u +_{0.0849h,0} u +_{0,-0.0849h} u +_{0,0.0849h} u)] \quad \text{(B.8)}$$

Thus we arrive at

$$\frac{c_h}{c} = \frac{1}{\sqrt{0.0023 k_h h}}[2.7302 + 0.0023(f_3(1) + f_4(1)) - 0.0065(f_3(0.9151) + f_4(0.9151)) + 0.0127(f_3(0.7344) + f_4(0.7344)) - 0.0290(f_3(0.5) + f_4(0.5)) + 0.0968(f_3(0.2656) + f_4(0.2656)) - 0.7587(f_3(0.0849) + f_4(0.0849))]^{1/2} \quad \text{(B.9)}$$

Fig. 4d shows the variation of the relative velocity in Eq. (B.9) for different angles of propagation.

7th order spectral element:

For this element, the **MÜ** term gives

$$0.0013\ h^2_{0,0}\ddot{u} \quad \text{(B.10)}$$

and the **KU** term is

$$c^2[2.7143_{0,0}u - 0.0013(_{-h,0}u +_{h,0} u +_{0,-h} u +_{0,h} u) + 0.0035(_{-0.9359h,0}u +_{0.9359h,0} u +_{0,-0.9359h} u +_{0,0.9359h} u) - 0.0062(_{-0.7959h,0}u +_{0.7959h,0} u +_{0,-0.7959h} u +_{0,0.7959h} u) + 0.0119(_{-0.6046h,0}u +_{0.6046h,0} u +_{0,-0.6046h} u +_{0,0.6046h} u) - 0.0277(_{-0.3954h,0}u +_{0.3954h,0} u +_{0,-0.3954h} u +_{0,0.3954h} u) + 0.0946(_{-0.2041h,0}u +_{0.2041h,0} u +_{0,-0.2041h} u +_{0,0.2041h} u) - 0.7533(_{-0.0641h,0}u +_{0.0641h,0} u +_{0,-0.0641h} u +_{0,0.0641h} u)] \quad \text{(B.11)}$$

such that

$$\frac{c_h}{c} = \frac{1}{\sqrt{0.0013 k_h h}}[2.7143 - 0.0013(f_3(1) + f_4(1)) + 0.0035(f_3(0.9359) + f_4(0.9359)) - 0.0062(f_3(0.7959) + f_4(0.7959)) + 0.0119(f_3(0.6046) + f_4(0.6046)) - 0.0277(f_3(0.3954) + f_4(0.3954)) + 0.0946(f_3(0.2041) + f_4(0.2041)) - 0.7533(f_3(0.0641) + f_4(0.0641))]^{1/2} \quad \text{(B.12)}$$

Fig. 4e shows the results using Eq. (B.12).

8th order spectral element:

The **MÜ** term gives

$$7.7160e - 04 h^2_{0,0}\ddot{u} \quad \text{(B.13)}$$

and the **KU** term is

$$c^2[2.7037_{0,0}u + 7.7160e - 04(_{-h\,0}u +_{h,0} u +_{0,-h} u +_{0,h} u) - 0.0021(_{-0.9499h,0}u +_{0.9499h,0} u +_{0,-0.9499h} u +_{0,0.9499h} u) + 0.0034(_{-0.8386h,0}u +_{0.8386h,0} u +_{0,-0.8386h} u +_{0,0.8386h} u) - 0.0059(_{-0.6816h,0}u +_{0.6816h,0} u +_{0,-0.6816h} u +_{0,0.6816h} u) + 0.0113(_{-0.5h,0}u +_{0.5h,0} u +_{0,-0.5h} u +_{0,0.5h} u) - 0.0269(_{-0.3184h,0}u +_{0.3184h,0} u +_{0,-0.3184h} u +_{0,0.3184h} u) + 0.0931(_{-0.1614h,0}u +_{0.1614h,0} u +_{0,-0.1614h} u +_{0,0.1614h} u) - 0.7497(_{-0.0501h,0}u +_{0.0501h,0} u +_{0,-0.0501h} u +_{0,0.0501h} u)] \quad \text{(B.14)}$$

hence

$$\frac{c_h}{c} = \frac{1}{\sqrt{7.7160e - 04 k_h h}}[2.7037 + 7.7160e - 04(f_3(1) + f_4(1)) - 0.0021(f_3(0.9499) + f_4(0.9499)) + 0.0034(f_3(0.8386) + f_4(0.8386)) - 0.0059(f_3(0.6816) + f_4(0.6816)) + 0.0113(f_3(0.5) + f_4(0.5)) - 0.0269(f_3(0.3184) + f_4(0.3184)) + 0.0931(f_3(0.1614) + f_4(0.1614)) - 0.7497(f_3(0.0501) + f_4(0.0501))]^{1/2} \quad \text{(B.15)}$$

with the results shown in Fig. 4f.

We used for all these computations double-precision arithmetic on the computer but report the results only to four digits.

References

[1] Komatitsch D, Tromp J. Introduction to the spectral element method for three-dimensional seismic wave propagation. Geophys. J. Int. 1999;139:806–22.
[2] Kudela P, Krawczuk M, Ostachowicz W. Wave propagation modelling in 1D structures using spectral finite elements. J. Sound Vib. 2007;300:88–100.
[3] Aagaard BT, Heaton TH, Hall JF. Dynamic earthquake ruptures in the presence of lithostatic normal stresses: implications for friction models and heat production. Bull. Seismol. Soc. Am. 2001;91:1765–96.
[4] Komatitsch D, Tromp J. Spectral-element simulations of global seismic wave propagation—I. Validation. Geophys. J. Int. 2002;149:390–412.
[5] Komatitsch D, Tromp J. Spectral-element simulations of global seismic wave propagation—II. Three-dimensional models, oceans, rotation and self-gravitation. Geophys. J. Int. 2002;150:303–18.
[6] Hori M. Introduction to Computational Earthquake Engineering. Imperial College Press; 2011.
[7] Kaneko Y, Ampuero JP, Lapusta N. Spectral-element simulations of long-term fault slip: effect of low-rigidity layers on earthquake-cycle dynamics. J. Geophys. Res.: Solid Earth 2011;116.
[8] Igel H. Computational Seismology: A Practical Introduction. Oxford University Press; 2017.
[9] Zakian P, Khaji N. A stochastic spectral finite element method for wave propagation analyses with medium uncertainties. Appl. Math. Model. 2018;63:84–108.
[10] Zakian P, Khaji N. A stochastic spectral finite element method for solution of faulting-induced wave propagation in materially random continua without explicitly modeled discontinuities. Comput. Mech. 2019;64:1017–48.
[11] Mullen R, Belytschko T. Dispersion analysis of finite element semidiscretizations of the two-dimensional wave equation. Int. J. Numer. Meth. Eng. 1982;18:11–29.
[12] Bathe KJ. Finite Element Procedures: Prentice Hall; 1996, 2nd edition KJ Bathe, Watertown, MA, 2014; also published by Higher Education Press China, 2016.
[13] Krenk S. Dispersion-corrected explicit integration of the wave equation. Comput. Methods Appl. Mech. Eng. 2001;191:975–87.
[14] Guddati MN, Yue B. Modified integration rules for reducing dispersion error in finite element methods. Comput. Methods Appl. Mech. Eng. 2004;193:275–87.
[15] Noh G, Bathe KJ. An explicit time integration scheme for the analysis of wave propagations. Comput. Struct. 2013;129:178–93.
[16] Noh G, Ham S, Bathe KJ. Performance of an implicit time integration scheme in the analysis of wave propagations. Comput. Struct. 2013;123:93–105.
[17] Kim KT, Zhang L, Bathe KJ. Transient implicit wave propagation dynamics with overlapping finite elements. Comput. Struct. 2018;199:18–33.
[18] Seriani G, Oliveira SP. Dispersion analysis of spectral element methods for elastic wave propagation. Wave Motion 2008;45:729–44.
[19] Ainsworth M, Wajid HA. Dispersive and Dissipative Behavior of the Spectral Element Method. SIAM J. Numer. Anal. 2009;47:3910–37.
[20] Antonietti PF, Mazzieri I, Quarteroni A, Rapetti F. Non-conforming high order approximations of the elastodynamics equation. Comput. Methods Appl. Mech. Eng. 2012;209–212:212–38.

[21] Melvin T, Staniforth A, Thuburn J. Dispersion analysis of the spectral element method. Q. J. R. Meteorolog. Soc. 2012;138:1934–47.
[22] Mazzieri I, Rapetti F. Dispersion analysis of triangle-based spectral element methods for elastic wave propagation. Numerical Algorithms. 2012;60:631–50.
[23] Ferroni A, Antonietti PF, Mazzieri I, Quarteroni A. Dispersion-dissipation analysis of 3-D continuous and discontinuous spectral element methods for the elastodynamics equation. Geophys. J. Int. 2017;211:1554–74.
[24] Kaveh A. Optimal Structural Analysis. second ed. Chichester, UK: John Wiley & Sons; 2006.
[25] Komatitsch D, Vilotte JP, Vai R, Castillo-Covarrubias JM, Sánchez-Sesma FJ. The spectral element method for elastic wave equations—application to 2-D and 3-D seismic problems. Int. J. Numer. Meth. Eng. 1999;45:1139–64.
[26] Mercerat ED, Vilotte JP, Sánchez-Sesma FJ. Triangular Spectral Element simulation of two-dimensional elastic wave propagation using unstructured triangular grids. Geophys. J. Int. 2006;166:679–98.
[27] Kaneko Y, Lapusta N, Ampuero JP. Spectral element modeling of spontaneous earthquake rupture on rate and state faults: effect of velocity-strengthening friction at shallow depths. J. Geophys. Res.: Solid Earth 2008;113.
[28] Witkowski W, Rucka M, Chróścielewski J, Wilde K. On some properties of 2D spectral finite elements in problems of wave propagation. Finite Elem. Anal. Des. 2012;55:31–41.
[29] Chai Y, Bathe KJ. Transient wave propagation in inhomogeneous media with enriched overlapping triangular elements. Comput. Struct. 2020;237:106273.
[30] Malakiyeh MM, Shojaee S, Bathe KJ. The Bathe time integration method revisited for prescribing desired numerical dissipation. Comput. Struct. 2019;212:289–98.
[31] Casadei F, Gabellini E, Fotia G, Maggio F, Quarteroni A. A mortar spectral/finite element method for complex 2D and 3D elastodynamic problems. Comput. Methods Appl. Mech. Eng. 2002;191:5119–48.
[32] Newmark NM. A method of computation for structural dynamics. J. Eng. Mech. Div. 1959;85:67–94.
[33] Chung J, Lee JM. A new family of explicit time integration methods for linear and non-linear structural dynamics. Int. J. Numer. Meth. Eng. 1994;37:3961–76.
[34] Hulbert GM, Chung J. Explicit time integration algorithms for structural dynamics with optimal numerical dissipation. Comput. Methods Appl. Mech. Eng. 1996;137:175–88.
[35] Zhai WM. Two simple fast integration methods for large-scale dynamic problems in engineering. Int. J. Numer. Meth. Eng. 1996;39:4199–214.
[36] Tchamwa B, Conway T, Wielgosz C. An accurate explicit direct time integration method for computational structural dynamics. ASME PVP 1999;398:77–84.
[37] Babuška I, Suri M. The p- and h-p versions of the finite element method, an overview. Comput. Methods Appl. Mech. Eng. 1990;80:5–26.
[38] Campion SD, Jarvis JL. An investigation of the implementation of the p-version finite element method. Finite Elem. Anal. Des. 1996;23:1–21.
[39] Zakian P, Khaji N. A novel stochastic-spectral finite element method for analysis of elastodynamic problems in the time domain. Meccanica 2016;51:893–920.
[40] Zakian P, Khaji N, Kaveh A. Graph theoretical methods for efficient stochastic finite element analysis of structures. Comput. Struct. 2017;178:29–46.
[41] Kim KT, Bathe KJ. Transient implicit wave propagation dynamics with the method of finite spheres. Comput. Struct. 2016;173:50–60.
[42] Galvez P, Ampuero JP, Dalguer LA, Somala SN, Nissen-Meyer T. Dynamic earthquake rupture modelled with an unstructured 3-D spectral element method applied to the 2011 M9 Tohoku earthquake. Geophys. J. Int. 2014;198:1222–40.
[43] Yue B, Guddati MN. Dispersion-reducing finite elements for transient acoustics. J. Acoust. Soc. Am. 2005;118:2132–41.
[44] Miklowitz J. The Theory of Elastic Waves and Waveguides. Elsevier Science; 1978.
[45] Kim KT, Bathe KJ. Accurate solution of wave propagation problems in elasticity. Comput. Struct. 2021;249:106502.